Вісник
Харківського
Національного
Університету
імені В. Н. Каразіна

СЕРІЯ «ХІМІЯ»
Вип. 41 (64)

Kharkiv University Bulletin
Chemical series. Issue 41 (64)

Харків Kharkiv
2023

Вісник містить статті, присвячені різним аспектам теоретичної хімії, хімічного аналізу, органічної хімії, спектроскопії, фізико-хімії розчинів та поверхневих явищ, електрохімії, хімічного матеріалознавства.

Для науковців і фахівців. Видання є фаховим в галузі хімічних наук. (Наказ Міністерства освіти і науки України № 1643 від 28.12.2019 року)

Затверджено до друку рішенням Вченої ради Харківського національного університету імені В.Н. Каразіна (протокол № 21 від 27 листопада 2023 р.)

Статті пройшли внутрішнє та зовнішнє рецензування.

Свідоцтво про державну реєстрацію КВ № 21563-11463Р від 27.07.2015.

The Chemical Series publishes papers devoted to various aspects of theoretical chemistry, chemical analysis, organic chemistry, inorganic chemistry, physical chemistry of solutions and surface phenomena, electrochemistry, materials chemistry. The bulletin is officially authorized by the Highest Attestation Commission of Ukraine to publish results of research submitted for PhD and ScD degrees.

Publication of this issue is approved by the Academic Council of V.N. Karazin Kharkiv National University (protocol № 21 from 27.11.2023).

All articles have been reviewed.

Certificate of state registration KB № 21563-11463P from 27.07.2015.

ЗМІСТ

CONTENTS

MOLECULAR DYNAMICS STUDY OF IMIDAZOLIUM IONIC LIQUIDS AND MOLECULAR SOLVENTS: INSIGHTS INTO MICROSTRUCTURE AND TRANSPORT PHENOMENA

D.S. Dudariev[*†,a], Y.V. Kolesnik[*,b], A. Idrissi[†,c], O.N. Kalugin[*,d]

[*]*V. N. Karazin Kharkiv National University, School of Chemistry, 4 Svobody sqr., Kharkiv, 61022 Ukraine*

[†]*University of Lille, CNRS UMR 8516 -LASIRe - Laboratoire Avancé de Spectroscopie pour les Interactions la Réactivité et l'environnement, 59000 Lille, France*

a) ✉ dimadudariev@gmail.com   ⓘ https://orcid.org/0000-0002-2556-8036
b) ✉ ykolesnik@karazin.ua   ⓘ https://orcid.org/0000-0002-9569-4556
c) ✉ nacer.idrissi@univ-lille1.fr   ⓘ https://orcid.org/0000-0002-6924-6434
d) ✉ onkalugin@gmail.com   ⓘ https://orcid.org/0000-0003-3273-9259

Binary mixtures composed of room-temperature ionic liquids and aprotic dipolar solvents are widely used in the modern electrochemistry. While these systems exhibit maximum electroconductivity and other changes in diluted solutions, as confirmed by NMR and vibrational spectroscopic data, there is currently no theory that can fully explain these phenomena. In current work twelve mixtures of ionic liquids (ILs), in particular 1-butyl-3-methylimdazolium (C_4mim^+) with tetrafluoroborate (BF_4^-), hexafluorophosphate (PF_6^-), trifluoromethanesulfonate (TFO^-) and bis(trifluoromethane)sulfonimide ($TFSI^-$) with molecular solvents such as acetonitrile (AN), propylene carbonate (PC) or gamma butyrolactone (γ-BL) were studied by the molecular dynamics simulation technique. The local structure of the mixtures was studied in the framework of radial distribution functions (RDFs) and running coordination numbers (RCNs) that showed the particular behavior in AN and $TFSI^-$ systems. For $TFSI^-$ system the presence of two peaks on the RDFs with similar intensities were observed. The mutual arrangement of cation and anion corresponding to observed on the RDFs interatomic distances were investigated: they represent the position when the nitrogen atom of the anion is close to the imidazolium ring and when nitrogen atom of TFSI- not directly interacting with the ring, but instead the oxygen atoms do. The cation-anion coordination numbers changed for mixtures with AN from ~1.2 to ~3.6, for PC – from 0.6 to 3.0 and for γ-BL – from 0.8 to 3.1 with the increasing mole fraction of the ILs. Also, the association analysis was conducted using two different distance criteria. The results showed the formation of large clusters at approximately 0.15, 0.20, and 0.25 IL mole fractions for AN, PC, and γ-BL, respectively, based on the first criterion. However, this criterion tends to overestimate the extent of aggregation. In contrast, the second, stricter criterion indicates that the formation of large aggregates begins at IL mole fractions similar to where the experimental conductivity curves reach their maximum. To analyze the transport properties the diffusion coefficients of all the components and shear viscosity for all binary mixtures were obtained. The diffusion coefficients show good agreement with experimental data.

Keywords: *1-butyl-3-methylimdazolium, ionic liquids, aprotic dipolar solvents, local structure, transport properties, ionic aggregation*

Introduction

Ionic liquid (IL) mixtures with molecular solvents can be considered as electrolyte solutions, for which their structure and properties are determined by the balance of types of interactions between all particles in the solution (cation, anion and solvent), which determine the existence of ionic associates and high-order aggregates . In this context, the main feature of binary systems based on IL is that the constituent ions are polyatomic and, as a rule, asymmetric. As a result, the interactions mentioned above should be considered as anisotropic, having a predominant localization around some molecular fragment (center of interaction) . Another important feature of these systems in comparison with ordinary solutions of electrolytes is the complete miscibility of IL with many molecular solvents, which makes it possible to obtain mixtures corresponding to either a solution of such a liquid in a molecular solvent or a solution of a molecular solvent in an ionic liquid.

Intermolecular interactions in mixtures of two liquids of different nature can be showed as a gradual transition from the "first pure liquid" to the "second pure liquid" through intermediate

compositions. Thus, the task boils down to the following question: which ranges of composition correspond to the above-mentioned areas, and which intermolecular interactions are decisive .

For pure ILs, there is currently no generally accepted picture of their structure due to the indirect nature of the methods used. It is widely believed that in the liquid state the structure of imidazolium ionic liquids is determined by strong interionic Coulomb interactions, which are relatively effectively shielded away from the central ion (i.e., are quite local). It is also assumed that a significant contribution is made by the three-dimensional network of hydrogen bonds between counterions . The strength and structure of this network are determined by the nature (polarizability, polarizing action, size, etc.) of the anion .

The above-mentioned considerations about the structure of pure components indicate the presence of two main phenomena in which a redistribution of the equilibrium between possible ion-ion, ion-molecular and intermolecular interactions can be manifested when the composition changes. These are ionic association and ionic solvation .

These phenomena can be explained as the gradual breakdown of large ionic aggregates, which are the fundamental structural units of pure ionic liquids, into smaller aggregates and eventually into ion pairs. This process occurs as the system transitions from a concentrated ionic liquid to a more dilute solution. In dilute solutions, ion pairs completely dissociate into "free" ions due to interactions with the solvent. These interactions can be specific, involving localized ion-molecular interactions, or non-specific, resulting from the presence of a large amount of solvent that creates an environment similar to that of a pure solvent. .

The phenomena of ionic association and solvation are manifested at the microscopic level in the redistribution of electron density in the corresponding areas of interaction and, therefore, in changes in the corresponding force constants. Among the currently known experimental methods that can detect such effects, NMR and vibrational (IR and Raman) spectroscopy should be singled out. The first can reveal information about the change in the electronic microenvironment of each chemically non-equivalent nucleus and the relative location for some nuclei, while the second investigates changes in the constants of the dipole moment, polarizability, changes in the microenvironment of atoms participating in the studied vibrational mode .

The association and solvation are also reflected in the "statistical" microstructure of such binary mixtures. Currently, only various methods of diffraction of X-rays and neutrons can provide experimental data on the such microstructure in different time and size scales. Also, they are quite expensive and not always available, as well as difficult from the point of view of data processing. As well, usually there is only one IL-solvent system under investigation which means that the approach for studying such objects should be wider and more universal. Molecular dynamics (MD) simulation can help solve these problems, and this method can also complete the picture with information not available from experiment .

In this work MD simulation of twelve mixtures of ILs (1-butyl-3-methylimdazolium (C_4mim^+) with tetrafluoroborate (BF_4^-), hexafluorophosphate (PF_6^-), trifluoromethanesulfonate (TFO^-) and bis(trifluoromethane)sulfonimide ($TFSI^-$)) with molecular solvents (acetonitrile (AN), propylene carbonate (PC) or gamma butyrolactone (γ-BL)) of six IL mole fractions were performed. The molecular structures of the objects are presented at Figure 1. The microstructure, clusterization and, finally, the transport properties of the systems have been studied.
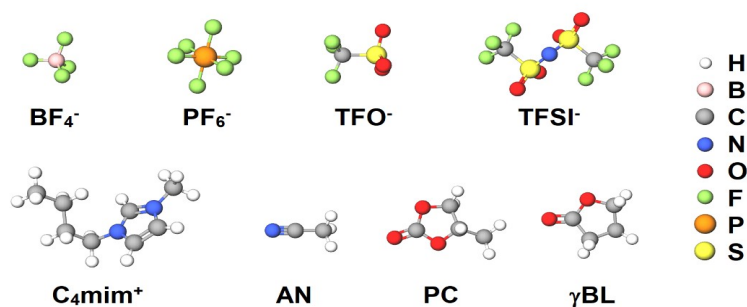
Figure 1. Structure of the ions and molecular solvents considered in this study

Methodology

Details of molecular dynamics simulation. MD simulations have been performed at the temperature of 298.15 K. To set the size of the cubic simulation box, a short (i.e., 1 ns) run has been performed on the isothermal-isobaric *NPT* ensemble at 1 bar. All simulations have been carried out using the GROMACS 2019.4 software package . The temperature and the pressure have been kept constant by means of the velocity-rescaling thermostat with the relaxation time of 0.1 ps, and the Berendsen barostat with the relaxation time of 0.5 ps, respectively. Equations of motion have been integrated using the leap-frog algorithm with a time-step of 0.5 fs. All interactions have been truncated to zero beyond the center-center cut-off distance of 1.2 nm. The long-range part of the electrostatic interaction has been accounted for by the particle mesh Ewald method , while that of the Lennard-Jones interaction has been treated by the conventional shifted force technique. The Lennard-Jones parameters corresponding to unlike pairs of atoms have been calculated by the standard Lorentz-Berthelot combination rules . After equilibrating the systems in the *NPT* ensemble, simulations of 10 ns have been performed in the *NVT* ensemble using the equilibrium density obtained from the constant pressure run. Each set of systems was simulated five times, starting from independently generated random configurations. These parallel calculations were then used to average the data for all structural and transport properties. The last 1 ns of the trajectories from these simulations were used for detailed structural analyses, while the full 10 ns trajectories were utilized for calculating transport properties.

The simulations of the binary mixtures (total of twelve systems) of four ILs of C_4mim^+ cation with different anions (BF_4^-, PF_6^-, TFO^- and $TFSI^-$) in three aprotic dipolar molecular solvents (AN, PC and γ-BL) have been performed. Six different compositions of the mole fraction of the ILs from 0.05 to 0.30 for each binary mixture were selected in a way that the total number of ion pairs for each composition was always equal to 100. The number of the different particles of the ILs in the simulated systems are collected in Table 1.

Table 1. Composition of the systems simulated.

IL mole fraction	Number of cations	Number of anions	Number of solvent molecules
0.05			1900
0.10			900
0.15			566
0.20	100	100	400
0.25			300
0.30			232

The ILs have been described by the potential model of Mondal and Balasubramanian [38-39], while for the solvent molecules the potential model of Koverga et al. [40-41] has been used. According to classical MD formalism, these potential models have the following functional form of the total potential energy:

$$U_{tot} = \sum_{ij}^{bonds} \frac{k_{r,ij}}{2}\left(r_{ij} - r_{0,ij}\right)^2 + \sum_{ijk}^{angles} \frac{k_{\theta,ijk}}{2}\left(\theta_{ijk} - \theta_{0,ijk}\right)^2 + \sum_{ijkl}^{dihedral} \sum_{n=0}^{5} C_n\left(\cos\left(\psi_{ijkl}\right)\right)^n +$$

$$+ \sum_{ij}^{nonbonded}\left(4\varepsilon_{ij}\left[\left(\frac{\sigma_{ij}}{r_{ij}}\right)^{12} - \left(\frac{\sigma_{ij}}{r_{ij}}\right)^6\right] + \frac{q_i q_j}{4\pi\varepsilon_0 r_{ij}}\right),$$

(1)

where k is the force constant for bond stretching (r), angle bending (θ), torsion (ϕ), respectively, ε and σ are the Lennard-Jones energy and the distance parameters, respectively, and q stands for the fractional charges of the interaction sites. For torsion angle $\psi_{ijkl} = 180^o - \phi_{ijkl}$. Indices i, j, k and l run through the interaction sites of the particles, while the subscript '0' refers to the equilibrium value of the bond lengths and angles. The potential model of ILs can be regarded a refinement of the CLaP force field [42-44]. Thus, while the bond and angle parameters have been retained, the torsional

parameters have been adapted to the Ryckaert-Bellemans analytical expression . Further, the charge distribution of the ions has been optimized in order to improve the agreement with the experimental thermodynamic and transport properties of the studied ILs. Thus, the ions of the IL carry a net charge that depends on the anion [38-39]. The potential models used here were previously validated by their ability of reproducing the basic experimental physicochemical properties of the systems [38-39].

Aggregate analysis. To study the association of ions, it is essential to establish a criterion by which two ions can be considered part of the same aggregate, cluster, or associate. Such a criterion was proposed in different works [46-47] as the distance between coordination centers of respective ions. Thus, two ions were considered to belong to the same associate if their respective centers are located at the equal or lower distance that was chosen as a criterion from each other .

After the definition of the criterion, the neighbor list of each cation and anion was determined for each configuration during the simulation at each timestep. The obtained neighbor list was later used to establish the connectivity between ions in the system. Important to note that mainly differently charged ions are coordinating around each other (anions around cations and vice versa). This means that the resulting clusters are constructed from the ions of altering charge that have the distance between them that fulfill the determined criterion.

Finally, the statistical analysis was applied to determine the characteristics of clusters. One of such statistical functions can be a size distribution of the aggregates $P(n)$. It shows the probability of finding an ion in an aggregate of size n:

$$P(n) = \frac{n\sum_{j=1}^{C} A_n(j)}{CN},$$
(2)

where $A_n(j)$ is the number of aggregates of size n for a given configuration j, C is the total number of configurations acquired during the simulation, N is the total number of cations and anions combined in the simulation box.

To better represent the results of the clusterization the average number of association $\bar{n}$ can be obtained. In general case, one can calculate it as follows:

$$\bar{n} = \sum_{i=1}^{N} n_i P_i(n)$$
(3)

Aggregate analysis has been performed by AGGREGATES 3.2.0 software package .

Transport properties. The coefficient of translational self-diffusion of atoms (molecules, ions) in a liquid can be found using the Green-Kubo relation:

$$D = \frac{1}{3}\int_0^\infty C_{vv}(t)\,dt.$$
(4)

For the viscosity a nonequilibrium periodic perturbation method has been used . To sum it up, molecular dynamic simulation is carried out in the 3D periodic cell with the external force in x direction $a(z)$. According to the Navier-Stokes's equation:

$$\rho\frac{\partial u}{\partial t} + \rho(u\cdot\nabla)u = \rho a - \nabla p + \eta\nabla^2 u,$$
(5)

where u is the velocity of the liquid, p is pressure of the fluid, ρ is the density of the fluid, t is time, η is viscosity. Because force is applied only in the x direction, the velocity along y and z will be zero:

$$\rho\frac{\partial u_x(z)}{\partial t} = \rho a_x(z) + \eta\frac{\partial^2 u_x(z)}{\partial z^2}.$$
(6)

The velocity profile as well as acceleration should be periodic because of the periodic system in the simulations. Thus, the cosine function can be used for this purpose:

$$a_x(z) = \Lambda\cos(kz),$$
(7)

$$k = \frac{2\pi}{l_z},$$
(8)

where l_z is the height of the box, Λ is the acceleration amplitude of the external force. The viscosity then can be obtained:

$$\eta = \frac{\Lambda}{V} \frac{\rho}{k^2}. \tag{9}$$

The measured viscosity greatly depends on the parameter Λ. To obtain the viscosity at zero acceleration few viscosities for different accelerations should be obtained. Then plotting the viscosities versus the amplitudes allows to obtain shear viscosity for $\Lambda=0$ via extrapolation.

Results and discussion

Structural properties. With the aim to study the cation-anion interaction, the interionic radial distribution functions (RDFs) and running coordination numbers (RCNs) of IL-solvent binary mixtures were analyzed. To fully consider these interactions the respective atoms for cations and anions should be chosen. Also, these points in space need to take into consideration all the coordination centers of cations and anions at once. For the C_4mim^+, the most positive charge is localized at the hydrogen sites around the imidazolium ring. Given this fact the center of the ring (CoR) is usually chosen as a reference point for the analysis [51-53]. Due to different structure, shape and symmetry of the anions their positions (X) for the analysis will be the follows: B atom in BF_4^-, P atom in PF_6^-, middle of the C-S bond in TFO^- (takes into account both O and F coordination sites) and N atom in $TFSI^-$ (takes into account N, O and F coordination sites).

The interionic RDFs for all IL-solvent binary mixtures for all simulated systems are shown in Figure 2.

Here the similar curves were obtained for all IL mole fractions, meaning the positions of the peaks and minima do not depend on the concentration of the IL. Furthermore, their positions do not vary at all for the same IL in different solvents. The first maxima for various anions occur at 0.49 nm (BF_4^-), 0.51 nm (PF_6^-) and 0.52 nm (TFO^-). For the $TFSI^-$ anion the situation is more complicated as there are two peaks at relatively low distances, 0.44 nm and 0.62 nm respectively. Also, these peaks have lower intensity comparing to other ILs. The first maximum in this case corresponds to the CoR-N interaction when N atom is located directly near the center of the ring or the H-atoms of the ring (the distances in both cases are similar). At the same time the second peak indicates the CoR-N interaction when N atom of $TFSI^-$ not directly interacting with the ring, but instead the oxygen atoms do. The example snapshot from the MD simulation trajectory files was obtained via VMD program package (Figure 3). These findings prove the quantum chemical calculations from the literature data . The first minima of RDFs for various anions are as follows: 0.70 nm (BF_4^-), 0.74 nm (PF_6^-), 0.73 nm (TFO^-) and 0.77 nm ($TFSI^-$). The behavior of the intensities of the peaks also changes in different ILs-solvent combinations. For all systems with AN the intensity becomes lower with the increasing of the ILs mole fraction. Also, for $TFSI^-$ system these changes are the lowest. Similar situation can be observed for all PC-containing systems where peak intensity do not change with the mole fraction of the ILs.
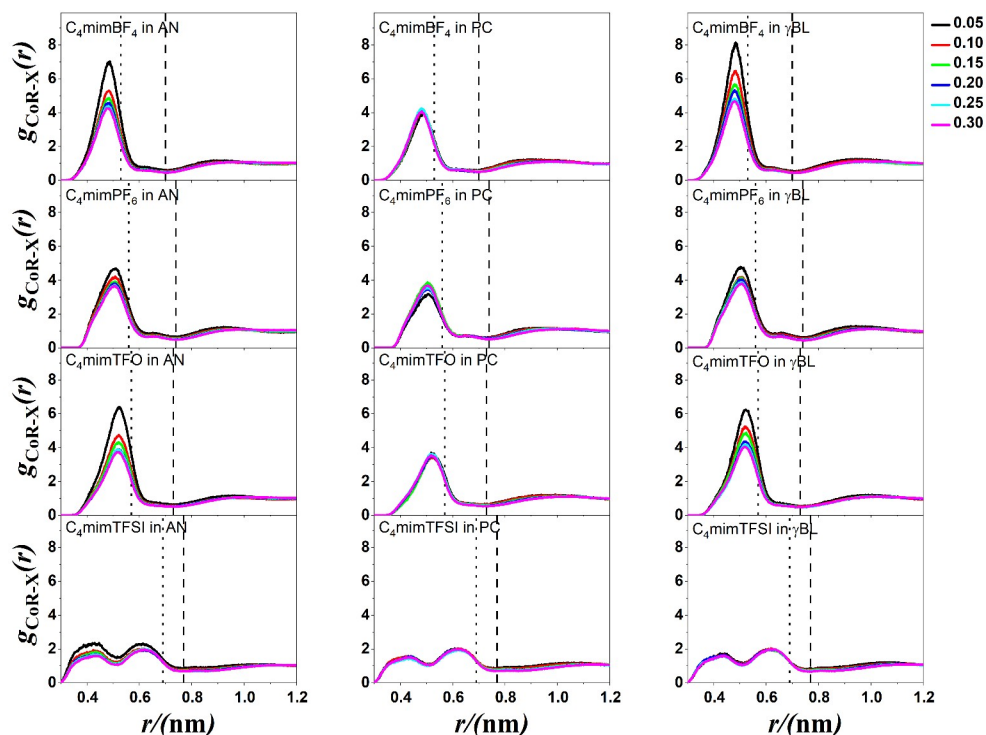
Figure 2. Cation-anion (CoR-X) radial distribution functions of the mixtures at various mole fraction of ionic liquid. The position of the cation is described with center of imidazolium ring. The positions of anions (X) are: B atom in BF_4^-, P atom in PF_6^-, middle of the C-S bond in TFO^- and N atom in $TFSI^-$. The vertical dashed and dotted lines correspond to the first and criterion, respectively, for aggregation analysis.
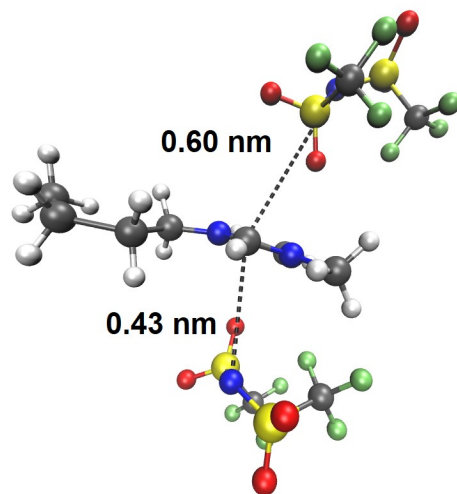
Figure 3. Example of $(C_4mim(TFSI)_2)^-$ associate in one of the $C_4mimTFSI$ system

The RCNs between cations and anions for all IL-solvent binary mixtures for all the systems simulated are presented in Figure 4.

11
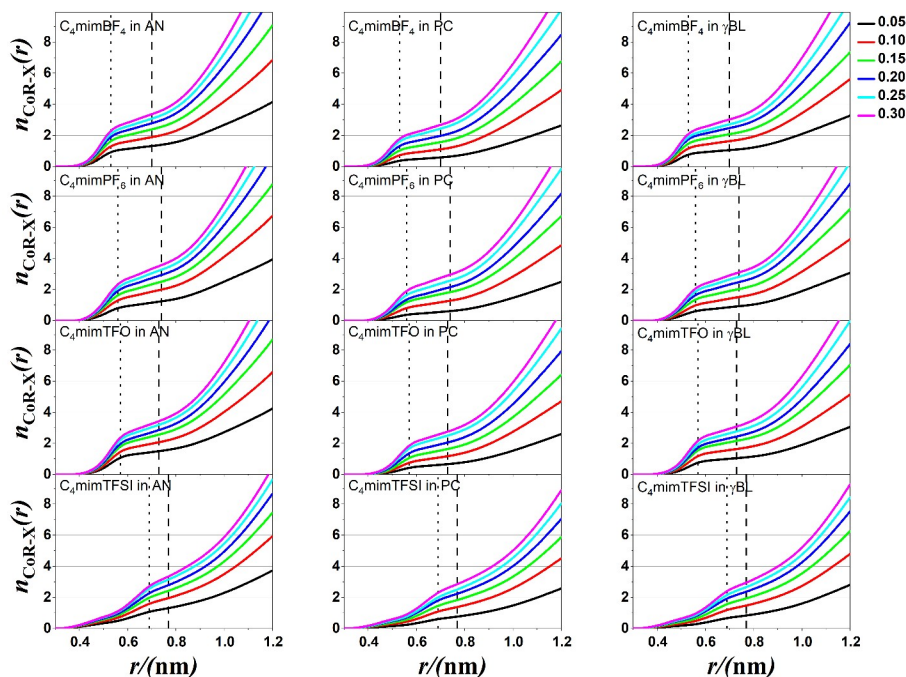
Figure 4. Cation-anion (CoR-X) running coordination numbers of the mixtures at various mole fraction of ionic liquid. The position of the cation is described with center of imidazolium ring. The positions of anions (X) are: B atom in BF_4^-, P atom in PF_6^-, middle of the C-S bond in TFO^- and N atom in $TFSI^-$. The vertical dashed and dotted lines correspond to the first and second criteria respectively, used for aggregation analysis.

The expected increase of the coordination number of the anion around the cation with the IL mole fraction increase can be observed at all of the graphs. The values of the coordination numbers however depend on the solvent. E.g., for AN it varies from ~1.2 (0.05 mole fraction of IL) to ~3.6 (0.30 mole fraction of IL), for PC – from 0.6 to 3.0 and for γ-BL – from 0.8 to 3.1 for all ILs. The coordination numbers of AN system being the biggest indicate the lowest among other solvent molecules dipole moment and as a result the weakest ion-solvent interaction in these systems, meaning with the ILs fraction increase the AN molecules are actively replaced with the anions in the cation first coordination sphere. Also, in the case of all $TFSI^-$ systems the curves values do not increase until at bigger distances.

Aggregate analysis. The ionic aggregates existence was analyzed via two different criteria. First criterion is the first minimum on the cation-anion RDF (Figure 2). This distance shows the border for the first coordination sphere where all of the anions are in strong interaction with the C_4mim^+ cation. As a second criterion the minimum on the second derivative of the RCN curve was proposed (Figure 5).
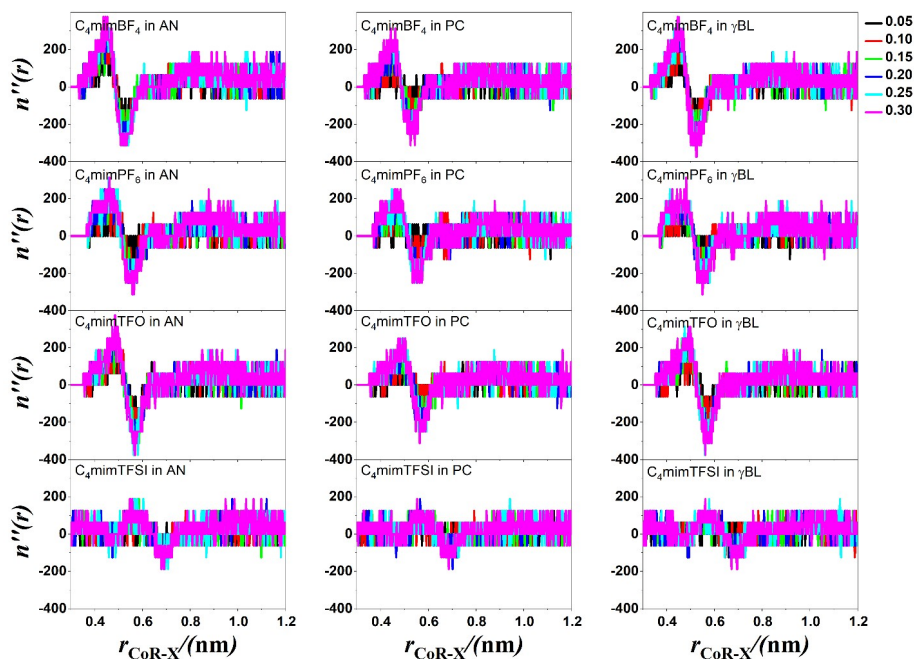
Figure 5. Second derivatives of the cation-anion (CoR-X) running coordination numbers of the mixtures at various mole fraction of ionic liquid. The position of the cation is described with center of imidazolium ring. The positions of anions are: B atom in BF_4^-, P atom in PF_6^-, middle of the C-S bond in TFO^- and N atom in $TFSI^-$.

This minimum marks the point where the RCN curve transitions to a plateau following an initial rapid increase. It is slightly shifted from the first peak in the RDF, or the second peak in systems containing the $TFSI^-$ anion, as explained in the previous section. The values of the distances for this criterion are next: 0.53 nm (BF_4^-), 0.56 nm (PF_6^-), 0.57 nm (TFO^-) and 0.69 nm ($TFSI^-$).

The results of the clusters formation probability for all mixtures of all mole fractions can be found in Figures 6-17 for the first and second criteria respectively.
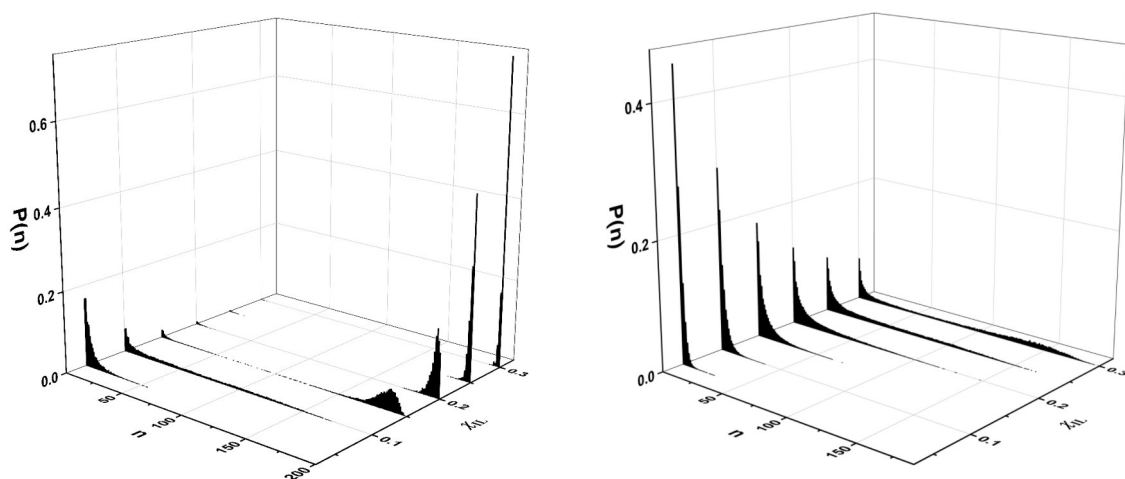
Figure 6. Probability distributions of aggregate sizes with first (left) and second (right) criterion of the C_4mimBF_4 in AN binary mixture at various mole fraction of ionic liquid.
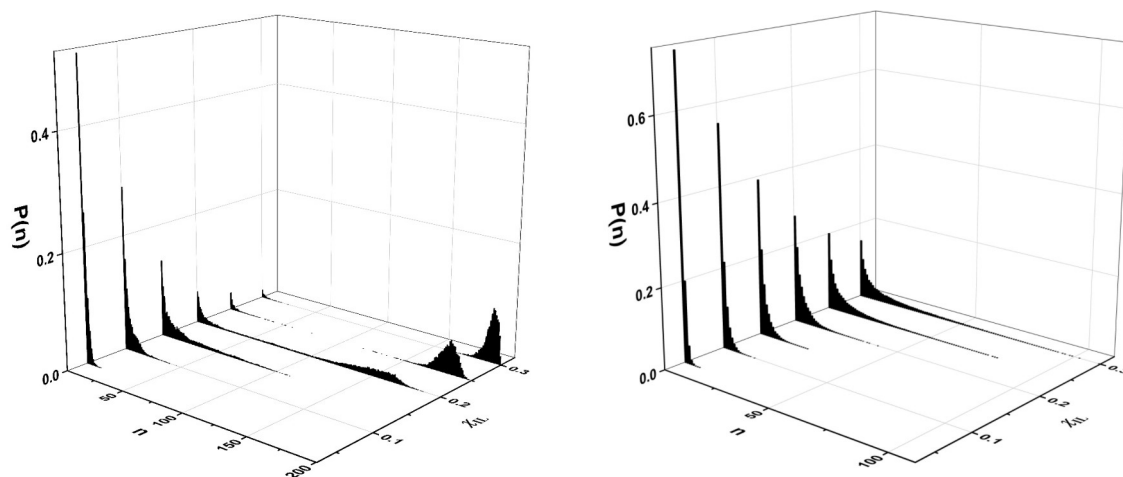
Figure 7. Probability distributions of aggregate sizes with first (left) and second (right) criterion of the C_4mimBF_4 in PC binary mixture at various mole fraction of ionic liquid.
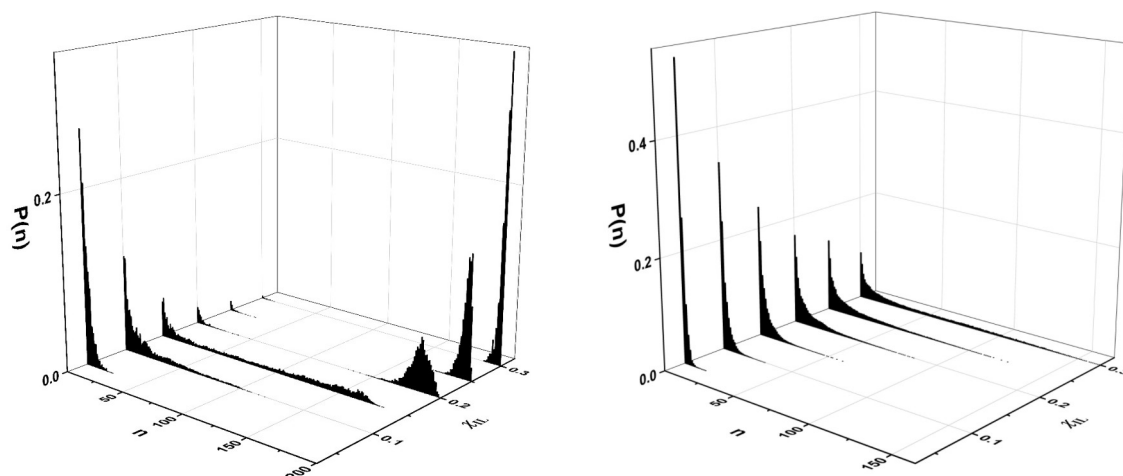
Figure 8. Probability distributions of aggregate sizes with first (left) and second (right) criterion of the C_4mimBF_4 in γ-BL binary mixture at various mole fraction of ionic liquid.
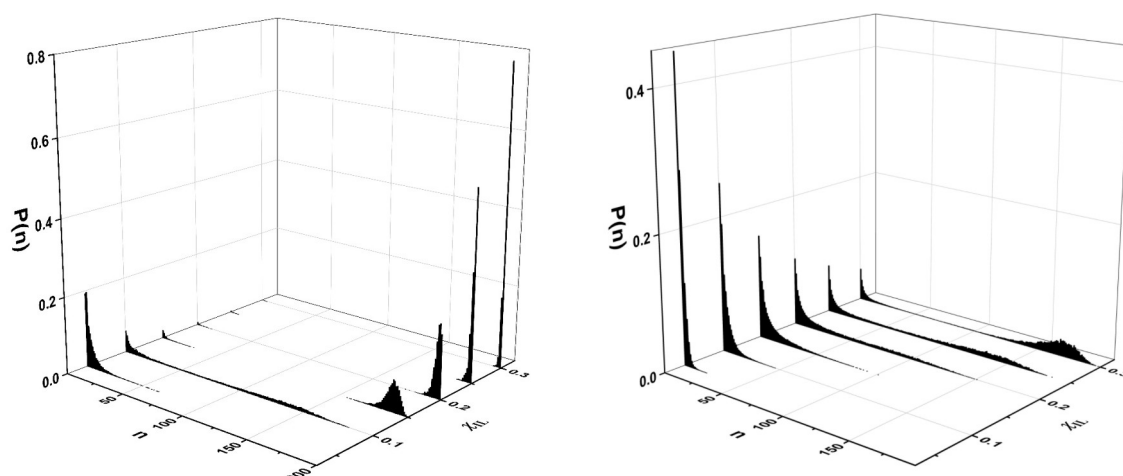
Figure 9. Probability distributions of aggregate sizes with first (left) and second (right) criterion of the C_4mimPF_6 in AN binary mixture at various mole fraction of ionic liquid.
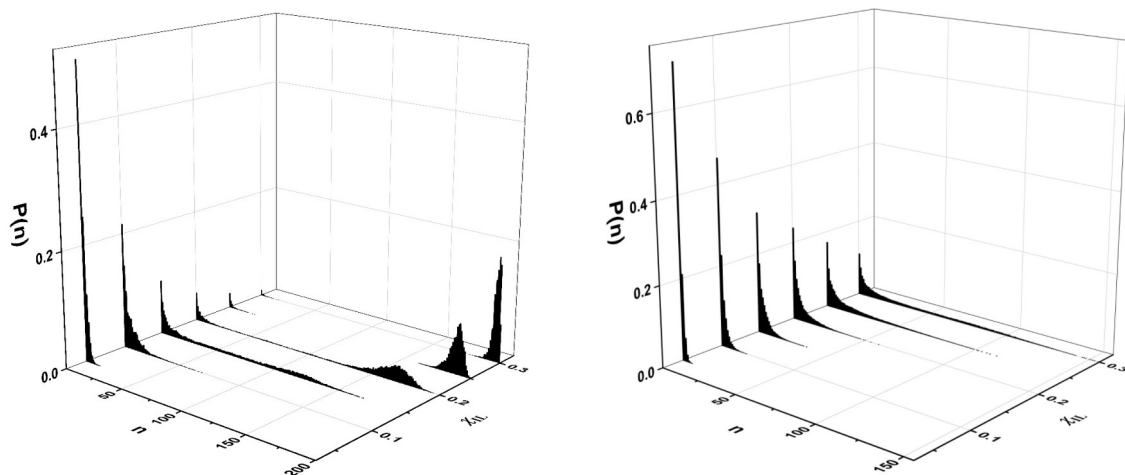
Figure 10. Probability distributions of aggregate sizes with first (left) and second (right) criterion of the C_4mimPF_6 in PC binary mixture at various mole fraction of ionic liquid.
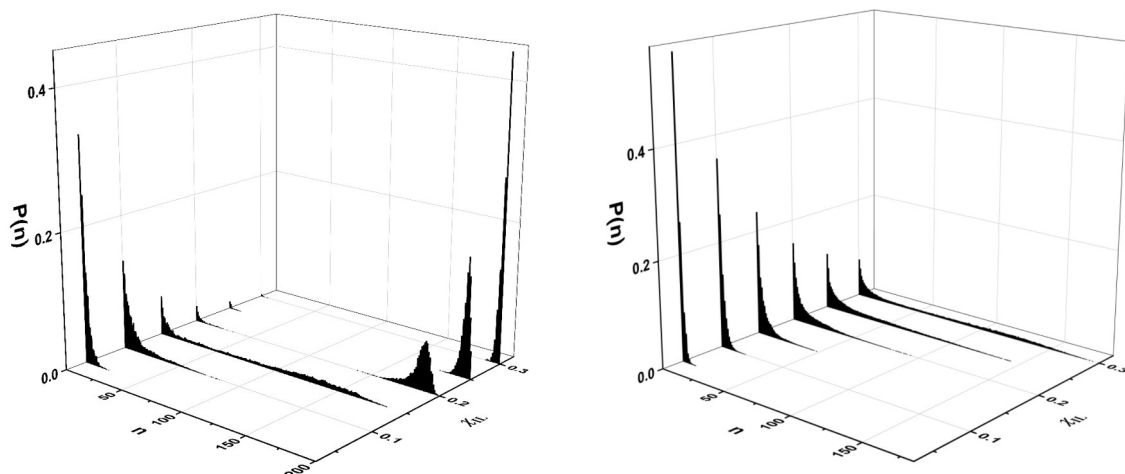
Figure 11. Probability distributions of aggregate sizes with first (left) and second (right) criterion of the C_4mimPF_6 in γ-BL binary mixture at various mole fraction of ionic liquid.
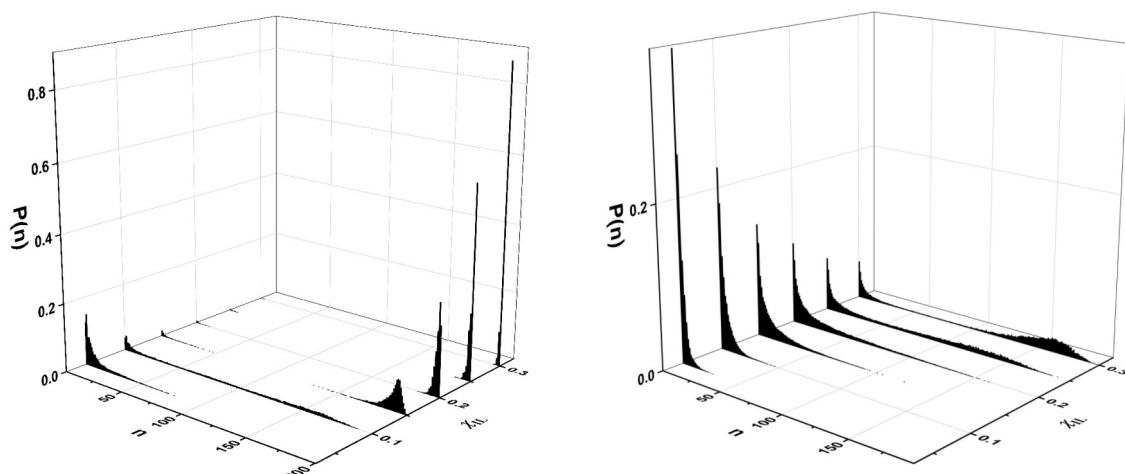
Figure 12. Probability distributions of aggregate sizes with first (left) and second (right) criterion of the $C_4mimTFO$ in AN binary mixture at various mole fraction of ionic liquid.
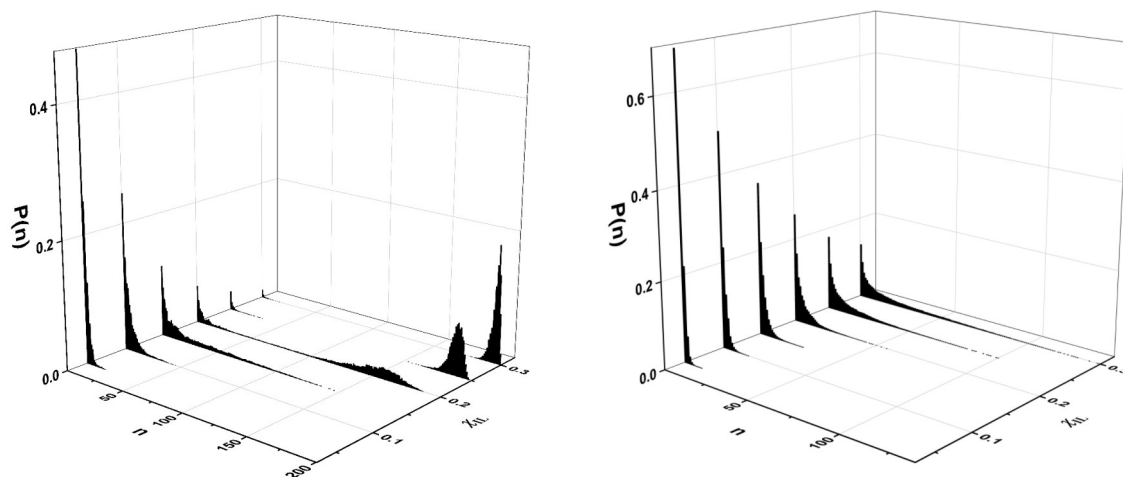
Figure 13. Probability distributions of aggregate sizes with first (left) and second (right) criterion of the C_4mimTFO in PC binary mixture at various mole fraction of ionic liquid.
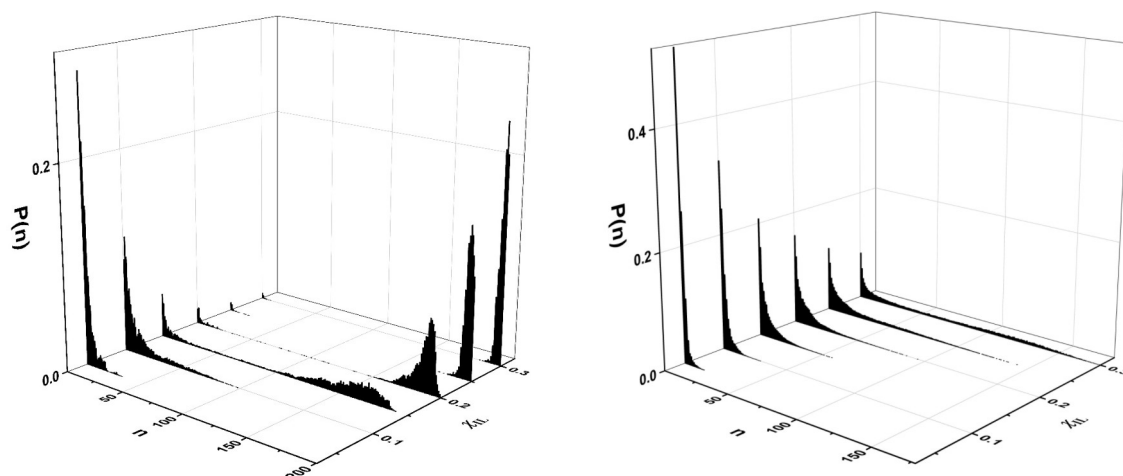
Figure 14. Probability distributions of aggregate sizes with first (left) and second (right) criterion of the C_4mimTFO in γ-BL binary mixture at various mole fraction of ionic liquid.
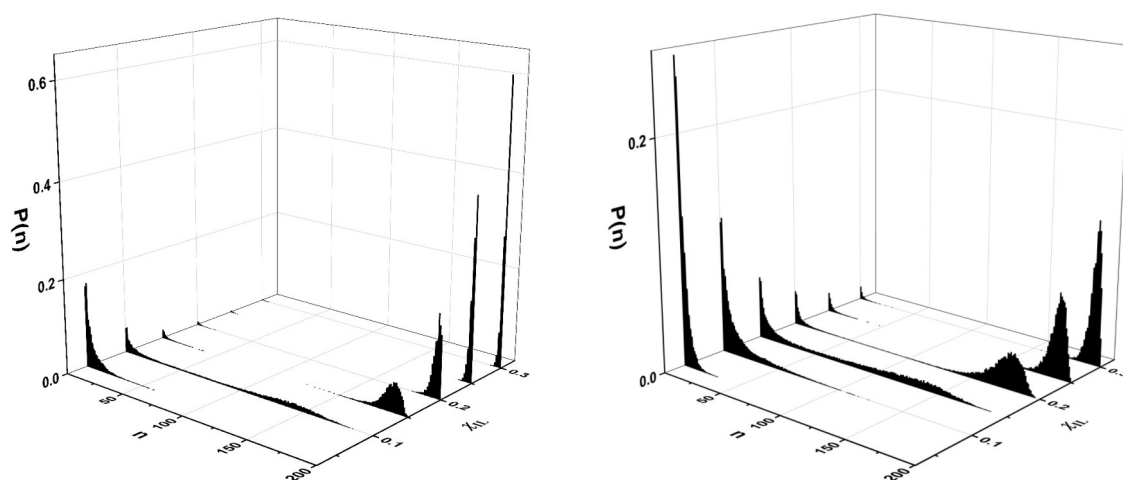
Figure 15. Probability distributions of aggregate sizes with first (left) and second (right) criterion of the C_4mimTFSI in AN binary mixture at various mole fraction of ionic liquid.
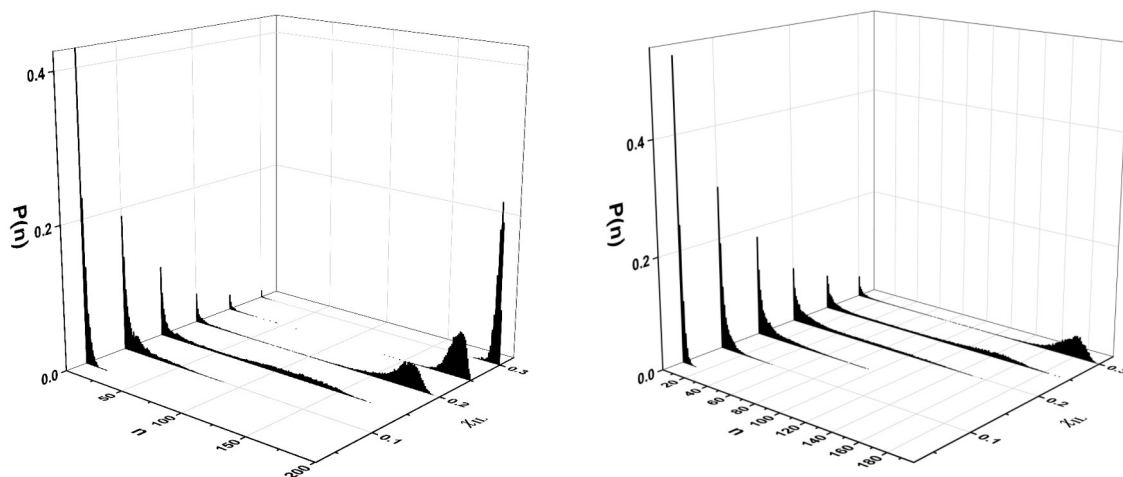
Figure 16. Probability distributions of aggregate sizes with first (left) and second (right) criterion of the C_4mimTFSI in PC binary mixture at various mole fraction of ionic liquid.
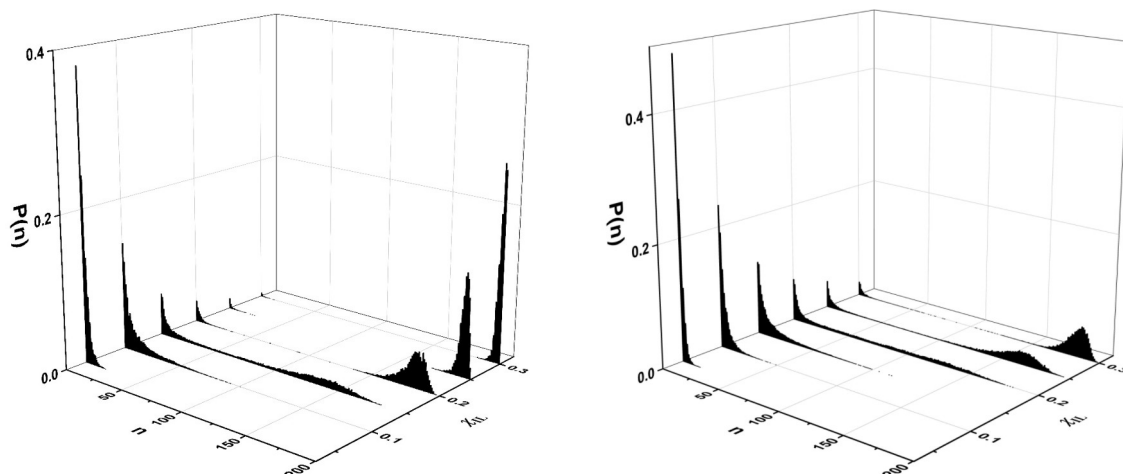
Figure 17. Probability distributions of aggregate sizes with first (left) and second (right) criterion of the C_4mimTFSI in γ-BL binary mixture at various mole fraction of ionic liquid.

The aggregates increase in size with the increasing of the IL mole fraction for each system. The small clusters are dominating in the most diluted systems when using the first criteria. As the mole fraction of IL increases up to 0.10 for AN mixtures, 0.15 for PC mixtures, and 0.20 for γ-BL mixtures, transition systems are formed in which a large number of aggregates of different types are present. With the further increase of mole fraction of the ILs all the systems start to form large aggregates that include most of the ions in the mixture can be observed. The existence of such huge continuous polar network, however, still allows small clusters or even isolated ions to exist in systems. Most probably these small aggregates lose the connectivity with the huge cluster, but their low probabilities of formation prove that it is a temporary phenomenon. At the highest observed concentration, nevertheless, the ions are part of one massive associate.

It shows that at the first distance criterion (minimum on the interionic RDF) the aggregate formation is overestimated in the mixture as there are no charge carriers left in this case and thus there should be no conductivity at these mole fraction of the ILs. However, the experimental results show otherwise [55-58].

As for the second criteria, it shows that transition to the massive association occurs only at the highest IL mole fraction of 0.30 (for TFSI⁻ – at 0.20-0.25). However, for the binary mixtures with AN the tendency for larger clusters formation appears at lower IL mole fraction compared to PC and γ-BL mixtures. This shows that AN demonstrates a weaker ion-solvent interaction, allowing ions at lower concentration form a continuous polar network regardless of the chosen criteria.

To better illustrate the clusterization processes the average numbers of associations were obtained for all systems (Figure 18). The figure displays in more compact way the same results that were discussed earlier. Here for the first criterion ions in AN systems form massive aggregates at 0.15 mole fraction of ILs already, in γ-BL and PC mixtures – at 0.20 and 0.25 respectively. For the second criterion the ions in the systems are separated from each other or forming small aggregates until ~0.15-0.20 mole fraction of the ILs. After that value of mole fraction ILs in mixtures tend to form bigger aggregates. For the BF$_4^-$, PF$_6^-$ and TFO$^-$ in PC this trend is not so pronounced. The massive aggregation process occurs only in TFSI$^-$ systems for the second criterion and only at highest concentration of 0.30. The AN systems at this concentration at the transition stage, however for the C$_4$mimTFSI in AN mixture almost all ions are part of the big associate even at the mole fraction of ILs of 0.25.
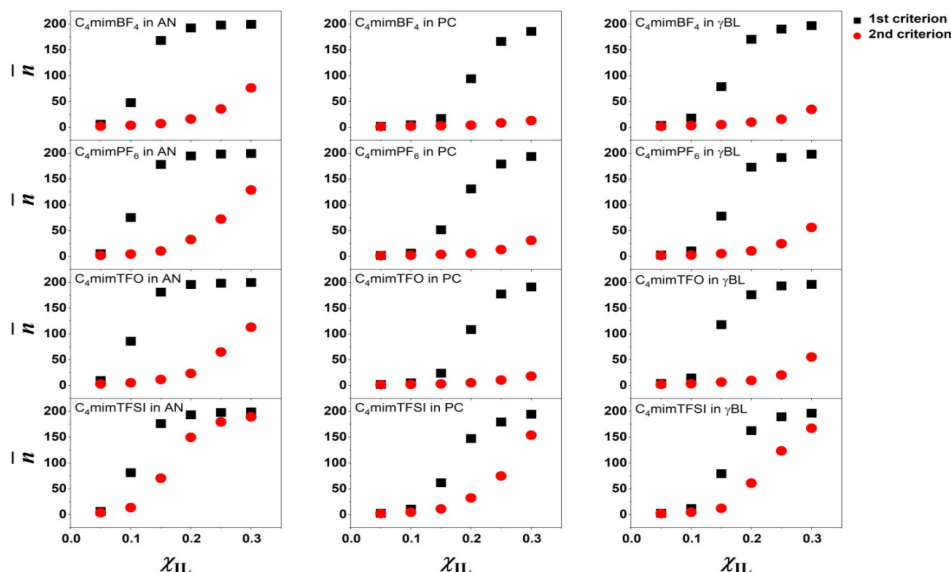
Figure 18. Average numbers of association with first minima on the RDFs (1st criteria) and with the minima on the second derivative on the RCN (2nd criteria) of the mixtures at various mole fraction of ionic liquid.

Nernst-Einstein relation postulates that conductivity depends on the concentration of the charge carriers in the solution :

$$\kappa = \frac{e^2}{Vk_BT}\left(N_+z_+^2\overline{D}_+ + N_-z_-^2\overline{D}_-\right) \tag{10}$$

where e is the elementary charge, k_B – Boltzmann constant, V – volume of the system, T – temperature of the system, $z_\pm$ – charge of the ion, $N_\pm$ – number of cations and anions.

Ionic aggregation reduces its concentration and effectively causes the drop in the conductivity value. As seen from the Figure 18, the mole fractions of rapid increase in the aggregates formation are the same as the conductivity maxima are located: at ~0.10 for AN systems and at ~0.20 for PC and γ-BL ones [55-58].

Transport properties. The diffusion coefficients and shear viscosities were obtained for all the IL mole fractions for all systems. The results are presented at Figures 19 and 20 respectively.
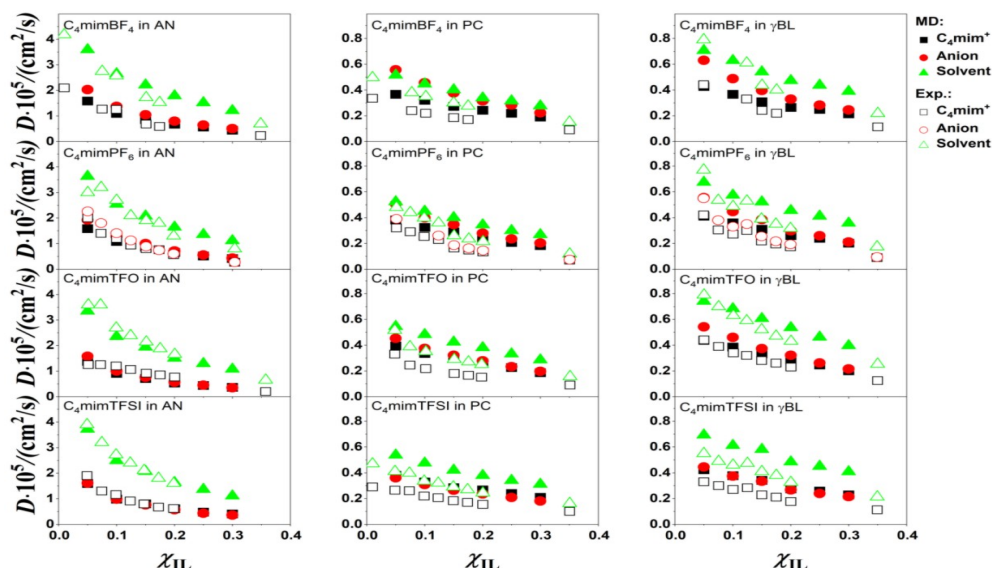
Figure 19. Diffusion coefficients for cation, anions and solvent molecules in comparison with the experimental data of the mixtures at various mole fraction of ionic liquid.

The diffusion coefficients were compared to the experimental data for cations and solvent molecules (and also for anions for the systems with PF_6^-) . For the binary mixtures with AN the obtained coefficients are very close to the experimental ones for all of the components of the analysis. For the systems with PC and γ-BL the obtained diffusion coefficients have in general higher values comparing to the experiment by 20%, especially for the higher concentrations.

For all systems the diffusion coefficients of the solvent molecules are higher than of the cation or anions, while the latter are close to each other for almost all systems and IL mole fractions. Also, the coefficients of the components in the systems with AN molecules are 3-5 times higher than with other two solvent molecules. For all PC systems the general trend is almost similar diffusion coefficient for anion and solvent molecule. For the C_4mimBF_4 in PC simulated system the anion diffusion coefficient is even higher in the most diluted solution. On the other hand, this behavior cannot be observed in the experimental data.
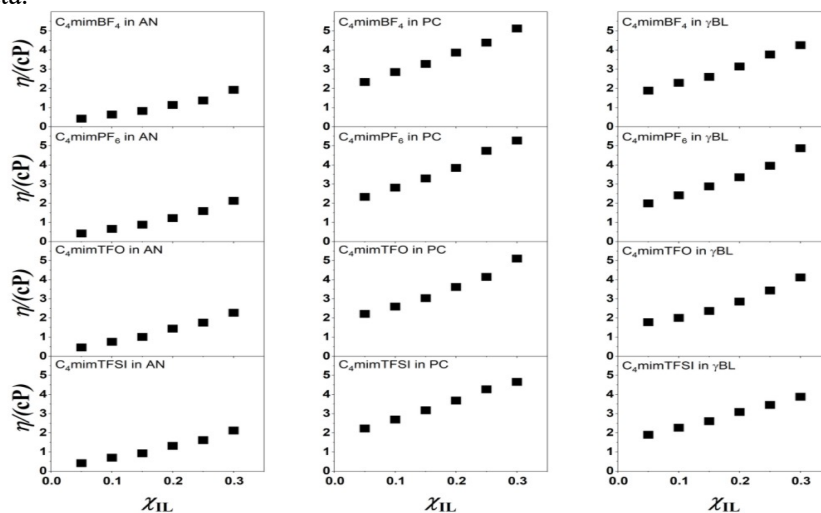
Figure 20. Viscosities of the mixtures at various mole fraction of ionic liquid

The viscosities at Figure 20 are increasing with the IL mole fraction increase by a non-linear dependance. Although, the values for all systems do not show any drastic changes at respective mole fractions where the experimental conductivity has maximum.

As the Nernst-Einstein relation shows (Equation 10), not only concentration of the charge carriers influence the conductivity but the diffusion coefficients as well . The behavior of calculated diffusion coefficients from the simulation for ions is in agreement with this statement.

Conclusions

In current work twelve ILs (C_4mim^+ with BF_4^-, PF_6^-, TFO^- and $TFSI^-$) with molecular solvents (acetonitrile, propylene carbonate, and gamma butyrolactone) binary mixtures were studied by the molecular dynamics simulation technique.

The microstructure of the mixtures was studied in the framework of radial distribution functions and running coordination numbers. The RDFs and RCNs show the particular behavior in AN and $TFSI^-$ systems. For TFSI- system the cation-anion (CoR-N) RDFs curves showed two peaks with similar intensities. It was shown that they represent the position when the nitrogen atom of the anion is close to the imidazolium ring and when nitrogen atom of $TFSI^-$ not directly interacting with the ring, but instead the oxygen atoms do. The cation-anion coordination numbers changed in similar values for the same ionic liquids in different solvents: for AN it varies from ~1.2 to ~3.6, for PC – from 0.6 to 3.0 and for γ-BL – from 0.8 to 3.1 with the increasing mole fraction of the ILs. Also, data obtained were used to conduct a quantitative aggregate analysis with two different distance criteria (first minimum of RDF and minimum of the second derivative of the RCN respectively) to compare the results with each other. The analysis with the first criterion shows the formation of the massive cluster at ~0.15, 0.20 and 0.25 IL mole fraction for AN and for with γ-BL respectively. Thus, this criterion seems to overrate the aggregation process in the mixtures. With the second, shorter distance criterion the formation of big aggregates in the systems starting to occur at the same mole fractions of the ILs where the experimental conductivity curves change their behavior and the maximum occurs. It proves that the reason of such drastic changes in the conductivity particular lies in the local structure of the ILs and solvent molecules.

To evaluate the transport properties, we obtained the diffusion coefficients for all components and the shear viscosity for all binary mixtures. The diffusion coefficients closely align with experimental data, demonstrating excellent accuracy, particularly for systems containing AN. Although the viscosity measurements did not reveal any distinct trends at the mole fraction range of ILs corresponding to the experimental conductivity maximum, these findings provide valuable insights into the complex interactions within these mixtures.

Acknowledgement

References

1. Dorbritz S., Ruth W., Kragl U. Investigation on aggregate formation of ionic liquids. *Advanced Synthesis & Catalysis* 2005, *347* (9), 1273-1279. https://doi.org/10.1002/adsc.200404352
2. Andanson J. M., Traïkia M., Husson P. Ionic association and interactions in aqueous methylsulfate alkyl-imidazolium-based ionic liquids. *The Journal of Chemical Thermodynamics* 2014, *77* 214-221. https://doi.org/10.1016/j.jct.2014.01.031
3. Bešter-Rogač M., Stoppa A., Hunger J., Hefter G., Buchner R. Association of ionic liquids in solution: A combined dielectric and conductivity study of [bmim][cl] in water and in acetonitrile. *Physical Chemistry Chemical Physics* 2011, *13* (39), 17588-17588. https://doi.org/10.1039/C1CP21371G
4. Jan R., Rather G. M., Bhat M. A. Association of ionic liquids in solution: Conductivity studies of [bmim][cl] and [bmim][pf6] in binary mixtures of acetonitrile + methanol. *Journal of Solution Chemistry* 2013, *42* (4), 738-745. https://doi.org/10.1007/s10953-013-9999-4
5. Hou J., Zhang Z., Madsen L. A. Cation/anion associations in ionic liquids modulated by hydration and ionic medium. *Journal of Physical Chemistry B* 2011, *115* (16), 4576-4582. https://doi.org/10.1021/jp1110899

6. Boruń A. Conductance and ionic association of selected imidazolium ionic liquids in various solvents: A review. *Journal of Molecular Liquids* 2019, *276* 214-224. https://doi.org/10.1016/j.molliq.2018.11.140

7. Lovelock K. R. J. Quantifying intermolecular interactions of ionic liquids using cohesive energy densities. *Royal Society Open Science* 2017, *4* (12), 171223-171223. https://doi.org/10.1098/rsos.171223

8. Fumino K., Reimann S., Ludwig R. Probing molecular interaction in ionic liquids by low frequency spectroscopy: Coulomb energy, hydrogen bonding and dispersion forces. *Physical Chemistry Chemical Physics* 2014, *16* (40), 21903-21929. https://doi.org/10.1039/C4CP01476F

9. Anderson J. L., Ding J., Welton T., Armstrong D. W. Characterizing ionic liquids on the basis of multiple solvation interactions. *Journal of the American Chemical Society* 2002, *124* (47), 14247-14254. https://doi.org/10.1021/ja028156h

10. Angenendt K., Johansson P. Ionic liquid structures from large density functional theory calculations using mindless configurations. *The Journal of Physical Chemistry C* 2010, *114* (48), 20577-20582. https://doi.org/10.1021/jp104961r

11. Xiong Z., Gao J., Zhang D., Liu C. Hydrogen bond network of 1-alkyl-3-methylimidazolium ionic liquids: A network theory analysis. *Journal of Theoretical and Computational Chemistry* 2012, *11* (3), 587-598. https://doi.org/10.1142/S0219633612500381

12. Niemann T., Strate A., Ludwig R., Zeng H. J., Menges F. S., Johnson M. A. Cooperatively enhanced hydrogen bonds in ionic liquids: Closing the loop with molecular mimics of hydroxy-functionalized cations. *Physical Chemistry Chemical Physics* 2019, *21* (33), 18092-18098. https://doi.org/10.1039/C9CP03300A

13. Le Donne A., Adenusi H., Porcelli F., Bodo E. Hydrogen bonding as a clustering agent in protic ionic liquids: Like-charge vs opposite-charge dimer formation. *ACS Omega* 2018, *3* (9), 10589-10600. https://doi.org/10.1021/acsomega.8b01615

14. Fumino K., Wulf A., Ludwig R. Hydrogen bonding in protic ionic liquids: Reminiscent of water. *Angewandte Chemie International Edition* 2009, *48* (17), 3184-3186. https://doi.org/10.1002/anie.200806224

15. Brela M. Z., Kubisiak P., Eilmes A. Understanding the structure of the hydrogen bond network and its influence on vibrational spectra in a prototypical aprotic ionic liquid. *Journal of Physical Chemistry B* 2018, *122* (41), 9527-9537. https://doi.org/10.1021/acs.jpcb.8b05839

16. Avent A. G., Chaloner P. A., Day M. P., Seddon K. R., Welton T. Evidence for hydrogen bonding in solutions of 1-ethyl-3-methylimidazolium halides, and its implications for room-temperature halogenoaluminate(iii) ionic liquids. *Journal of the Chemical Society, Dalton Transactions* 1994, (23), 3405-3405. https://doi.org/10.1039/DT9940003405

17. Marekha B. A., Kalugin O. N., Bria M., Idrissi A. Probing structural patterns of ion association and solvation in mixtures of imidazolium ionic liquids with acetonitrile by means of relative [1]h and [13]c nmr chemical shifts. *Physical Chemistry Chemical Physics* 2015, *17* (35), 23183-23194. https://doi.org/10.1039/C5CP02748A

18. Bester-Rogac M., Stoppa A., Buchner R. Ion association of imidazolium ionic liquids in acetonitrile. *J Phys Chem B* 2014, *118* (5), 1426-35. https://doi.org/10.1021/jp412344a

19. Yalcin D., Drummond C. J., Greaves T. L. Solvation properties of protic ionic liquids and molecular solvents. *Physical Chemistry Chemical Physics* 2019, *22* (1), 114-128. https://doi.org/10.1039/C9CP05711K

20. Sadeghi R., Ebrahimi N. Ionic association and solvation of the ionic liquid 1-hexyl-3- methylimidazolium chloride in molecular solvents revealed by vapor pressure osmometry, conductometry, volumetry, and acoustic measurements. *Journal of Physical Chemistry B* 2011, *115* (45), 13227-13240. https://doi.org/10.1021/jp2055188

21. Dupont J. On the solid, liquid and solution structural organization of imidazolium ionic liquids. *Journal of the Brazilian Chemical Society* 2004, *15* (3), 341-350. https://doi.org/10.1590/S0103-50532004000300002

22. Zhao Y., Gao S., Wang J., Tang J. Aggregation of ionic liquids [cnmim]br (n = 4, 6, 8, 10, 12) in d2o: A nmr study. *Journal of Physical Chemistry B* 2008, *112* (7), 2031-2039. https://doi.org/10.1021/jp076467e

23. Tokuda H., Baek S. J., Watanabe M. Room-temperature ionic liquid-organic solvent mixtures: Conductivity and ionic association. *Electrochemistry* 2005, *73* (8), 620-622. https://doi.org/10.5796/electrochemistry.73.620

24. Richardson P. M., Voice A. M., Ward I. M. Pulsed-field gradient nmr self diffusion and ionic conductivity measurements for liquid electrolytes containing libf4 and propylene carbonate. *Electrochimica Acta* 2014, *130* 606-618. https://doi.org/10.1016/j.electacta.2014.03.072

25. Burrell G. L., Burgar I. M., Gong Q., Dunlop N. F., Separovic F. Nmr relaxation and self-diffusion study at high and low magnetic fields of ionic association in protic ionic liquids. *Journal of Physical Chemistry B* 2010, *114* (35), 11436-11443. https://doi.org/10.1021/jp105087n

26. Kundu K., Chandra G. K., Umapathy S., Kiefer J. Spectroscopic and computational insights into the ion-solvent interactions in hydrated aprotic and protic ionic liquids. *Physical Chemistry Chemical Physics* 2019, *21* (37), 20791-20804. https://doi.org/10.1039/C9CP03670A

27. Danten Y., Cabaço M. I., Besnard M. Interaction of water diluted in 1-butyl-3-methyl imidazolium ionic liquids by vibrational spectroscopy modeling. *Journal of Molecular Liquids* 2010, *153* (1), 57-66. https://doi.org/10.1016/j.molliq.2009.07.001

28. Marcus Y., Hefter G. Ion pairing. *Chemical Reviews* 2006, *106* (11), 4585-4621. https://doi.org/10.1021/cr040087x

29. Shimomura T., Takamuku T., Yamaguchi T. Clusters of imidazolium-based ionic liquid in benzene solutions. *The Journal of Physical Chemistry B* 2011, *115* (26), 8518-8527. https://doi.org/10.1021/jp203422z

30. Russina O., Sferrazza A., Caminiti R., Triolo A. Amphiphile meets amphiphile: Beyond the polar–apolar dualism in ionic liquid/alcohol mixtures. *The Journal of Physical Chemistry Letters* 2014, *5* (10), 1738-1742. https://doi.org/10.1021/jz500743v

31. Marekha B. A., Koverga V. A., Chesneau E., Kalugin O. N., Takamuku T., Jedlovszky P., Idrissi A. Local structure in terms of nearest-neighbor approach in 1-butyl-3-methylimidazolium-based ionic liquids: Md simulations. *The Journal of Physical Chemistry B* 2016, *120* (22), 5029-5041. https://doi.org/10.1021/acs.jpcb.6b04066

32. Zahn S., Brehm M., Brüssel M., Hollóczki O., Kohagen M., Lehmann S., Malberg F., Pensado A. S., Schöppke M., Weber H., et al. Understanding ionic liquids from theoretical methods. *Journal of Molecular Liquids* 2014, *192* 71-76. https://doi.org/10.1016/j.molliq.2013.08.015

33. Abraham M. J., Murtola T., Schulz R., Páll S., Smith J. C., Hess B., Lindah E. Gromacs: High performance molecular simulations through multi-level parallelism from laptops to supercomputers. *SoftwareX* 2015, *1-2* 19-25. https://doi.org/10.1016/j.softx.2015.06.001

34. Bussi G., Donadio D., Parrinello M. Canonical sampling through velocity rescaling. *The Journal of Chemical Physics* 2007, *126* (1), 014101. https://doi.org/10.1063/1.2408420

35. Berendsen H. J. C., Postma J. P. M., Van Gunsteren W. F., Dinola A., Haak J. R. Molecular dynamics with coupling to an external bath. *The Journal of Chemical Physics* 1998, *81* (8), 3684-3684. https://doi.org/10.1063/1.448118

36. Essmann U., Perera L., Berkowitz M. L., Darden T., Lee H., Pedersen L. G. A smooth particle mesh ewald method. *The Journal of Chemical Physics* 1998, *103* (19), 8577-8577. https://doi.org/10.1063/1.470117

37. Allen P., Tildesley D. J. *Computer simulation of liquids*. Clarendon Press: Oxford, 1987. https://doi.org/10.1093/oso/9780198803195.001.0001

38. Mondal A., Balasubramanian S. Quantitative prediction of physical properties of imidazolium based room temperature ionic liquids through determination of condensed phase site charges: A refined force field. *Journal of Physical Chemistry B* 2014, *118* (12), 3409-3422. https://doi.org/10.1021/jp500296x

39. Mondal A., Balasubramanian S. A refined all-atom potential for imidazolium-based room temperature ionic liquids: Acetate, dicyanamide, and thiocyanate anions. *Journal of Physical Chemistry B* 2015, *119* (34), 11041-11051. https://doi.org/10.1021/acs.jpcb.5b02272

40. Koverga V. A., Korsun O. M., Kalugin O. N., Marekha B. A., Idrissi A. A new potential model for acetonitrile: Insight into the local structure organization. *Journal of Molecular Liquids* 2017, *233* 251-261. https://doi.org/10.1016/j.molliq.2017.03.025

41. Koverga V. A., Voroshylova I. V., Smortsova Y., Miannay F. A., Cordeiro M. N. D. S., Idrissi A., Kalugin O. N. Local structure and hydrogen bonding in liquid γ-butyrolactone and propylene car-

bonate: A molecular dynamics simulation. *Journal of Molecular Liquids* 2019, *287* 110912-110912. https://doi.org/10.1016/j.molliq.2019.110912

42. Canongia Lopes J. N., Deschamps J., Pádua A. A. H. Modeling ionic liquids using a systematic all-atom force field. *The Journal of Physical Chemistry B* 2004, *108* (6), 2038-2047. https://doi.org/10.1021/jp0362133

43. Canongia Lopes J. N., Pádua A. A. H. Molecular force field for ionic liquids composed of triflate or bistriflylimide anions. *The Journal of Physical Chemistry B* 2004, *108* (43), 16893-16898. https://doi.org/10.1021/jp0476545

44. Canongia Lopes J. N., Pádua A. A. H. Molecular force field for ionic liquids iii: Imidazolium, pyridinium, and phosphonium cations; chloride, bromide, and dicyanamide anions. *The Journal of Physical Chemistry B* 2006, *110* (39), 19586-19592. https://doi.org/10.1021/jp063901o

45. Ryckaert J. P., Bellemans A. Molecular dynamics of liquid n-butane near its boiling point. *Chemical Physics Letters* 1975, *30* (1), 123-125. https://doi.org/10.1016/0009-2614(75)85513-8

46. Bernardes C. E. S., Minas da Piedade M. E., Canongia Lopes J. N. The structure of aqueous solutions of a hydrophilic ionic liquid: The full concentration range of 1-ethyl-3-methylimidazolium ethylsulfate and water. *The Journal of Physical Chemistry B* 2011, *115* (9), 2067-2074. https://doi.org/10.1021/jp1113202

47. Hanke C. G., Lynden-Bell R. M. A simulation study of water−dialkylimidazolium ionic liquid mixtures. *The Journal of Physical Chemistry B* 2003, *107* (39), 10873-10878. https://doi.org/10.1021/jp034221d

48. Marekha B. A., Kalugin O. N., Idrissi A. Non-covalent interactions in ionic liquid ion pairs and ion pair dimers: A quantum chemical calculation analysis. *Physical Chemistry Chemical Physics* 2015, *17* (26), 16846-16857. https://doi.org/10.1039/C5CP02197A

49. Bernardes C. E. S. Aggregates: Finding structures in simulation results of solutions. *J. Comput. Chem.* 2017, *38* (10), 753-765. https://doi.org/10.1002/jcc.24735

50. Hess B. Determining the shear viscosity of model liquids from molecular dynamics simulations. *The Journal of Chemical Physics* 2002, *116* (1), 209-209. https://doi.org/10.1063/1.1421362

51. Macchieraldo R., Esser L., Elfgen R., Voepel P., Zahn S., Smarsly B. M., Kirchner B. Hydrophilic ionic liquid mixtures of weakly and strongly coordinating anions with and without water. *ACS Omega* 2018, *3* (8), 8567-8582. https://doi.org/10.1021/acsomega.8b00995

52. Weber H., Hollóczki O., Pensado A. S., Kirchner B. Side chain fluorination and anion effect on the structure of 1-butyl-3-methylimidazolium ionic liquids. *The Journal of Chemical Physics* 2013, *139* (8), 084502-084502. https://doi.org/10.1063/1.4818540

53. Doherty B., Zhong X., Gathiaka S., Li B., Acevedo O. Revisiting opls force field parameters for ionic liquid simulations. *Journal of Chemical Theory and Computation* 2017, *13* (12), 6131-6145. https://doi.org/10.1021/acs.jctc.7b00520

54. Humphrey W., Dalke A., Schulten K. Vmd: Visual molecular dynamics. *Journal of Molecular Graphics* 1996, *14* (1), 33-38. https://doi.org/10.1016/0263-7855(96)00018-5

55. Kalugin O. N., Voroshylova I. V., Riabchunova A. V., Lukinova E. V., Chaban V. V. Conductometric study of binary systems based on ionic liquids and acetonitrile in a wide concentration range. *Electrochimica Acta* 2013, *105* 188-199. https://doi.org/10.1016/j.electacta.2013.04.140

56. Vraneš M., Papović S., Tot A., Zec N., Gadžurić S. Density, excess properties, electrical conductivity and viscosity of 1-butyl-3-methylimidazolium bis(trifluoromethylsulfonyl)imide + γ-butyrolactone binary mixtures. *The Journal of Chemical Thermodynamics* 2014, *76* 161-171. https://doi.org/10.1016/j.jct.2014.03.025

57. Stoppa A., Hunger J., Buchner R. Conductivities of binary mixtures of ionic liquids with polar solvents. *Journal of Chemical & Engineering Data* 2009, *54* (2), 472-479. https://doi.org/10.1021/je800468h

58. Fu Y., Cui X., Zhang Y., Feng T., He J., Zhang X., Bai X., Cheng Q. Measurement and correlation of the electrical conductivity of the ionic liquid [bmim][tfsi] in binary organic solvents. *Journal of Chemical & Engineering Data* 2018, *63* (5), 1180-1189. https://doi.org/10.1021/acs.jced.7b00646

59. France-Lanord A., Grossman J. C. Correlations from ion pairing and the nernst-einstein equation. *Phys Rev Lett* 2019, *122* (13), 136001. https://doi.org/10.1103/PhysRevLett.122.136001

60. Marekha B. A., Kalugin O. N., Bria M., Buchner R., Idrissi A. Translational diffusion in mixtures of imidazolium ils with polar aprotic molecular solvents. *The Journal of Physical Chemistry B* 2014, *118* (20), 5509-5517. https://doi.org/10.1021/jp501561s

Д.С. Дударєв [*][†], Я.В. Колесник[*], А. Ідріссі[†], О.М. Калугін[*]. Молекулярно-динамічне дослідження іонних рідин на основі імідазолію та молекулярних розчинників: мікроструктура та транспортні властивості

[*]Харківський національний університет імені В.Н. Каразіна, хімічний факультет, майдан Свободи, 4, Харків, 61022, Україна

[†]Університет Лілю, CNRS UMR 8516 -LASIRe - Laboratoire Avancé de Spectroscopie pour les Interactions la Réactivité et l'environnement, 59000 Лілль, Франція

Бінарні суміші, що складаються з іонних рідин при кімнатній температурі та апротонних диполярних розчинників, широко використовуються в сучасній електрохімії. Хоча ці системи демонструють максимуми електропровідності та інші особливості в розведених розчинах, підтверджені даними ЯМР і вібраційної спектроскопії, на сьогоднішній день відсутня теорія, яка могла б пояснити ці явища. У даній роботі методом молекулярно-динамічного моделювання досліджено дванадцять сумішей іонних рідин (IP) зокрема 1-бутил-3-метилімдазолію (C_4mim^+) з тетрафлуорборатом (BF_4^-), гексафлуорфосфатом (PF_6^-), трифлуорметансульфонатом (TFO^-) і біс(трифлуорметан)сульфонімідом ($TFSI^-$)), у поєднанні з молекулярними розчинниками, такими як ацетонітрил (AN), пропіленкарбонат (PC) або гамма-бутиролактон (γ-BL). Локальну структуру сумішей досліджували за допомогою функцій радіального розподілу (ФРР) та поточних координаційних чисел (ПКЧ), що виявили особливості поведінки в системах з AN та $TFSI^-$. Для системи з $TFSI^-$ спостерігалися два піки на ФРР з однаковою інтенсивністю. Було досліджено взаємне розташування катіонів та аніонів, яке відповідає міжатомним відстаням, що спостерігаються на ФРР: вони відображають конфігурації, коли атом азоту аніону знаходиться поблизу імідазолієвого кільця, і коли атом азоту $TFSI^-$ безпосередньо не взаємодіє з кільцем, натомість це роблять атоми кисню. Катіон-аніонні координаційні числа змінювалися для сумішей з AN від ~1,2 до ~3,6, для PC – від 0,6 до 3,0 та для γ-BL – від 0,8 до 3,1 зі збільшенням молярної частки IP. Крім того, аналіз асоціації був проведений з використанням двох різних критеріїв відстані. Результати показали утворення великих кластерів при приблизно 0,15, 0,20 та 0,25 мольних частках іонної рідини для AN, PC та γ-BL відповідно, на основі першого критерію. Однак цей критерій має тенденцію переоцінювати ступінь агрегації. На відміну від нього, другий, суворіший критерій вказує, що утворення великих агрегатів починається при мольних частках іонної рідини, подібних до тих, де експериментальні криві провідності досягають максимуму. Для аналізу транспортних властивостей були отримані коефіцієнти дифузії всіх компонентів та в'язкість для всіх бінарних сумішей. Коефіцієнти дифузії добре узгоджуються з експериментальними даними.

Ключові слова:*. 1-бутил-3-метилімдазолій, іонні рідини, апротонні диполярні розчинники, локальна структура, транспортні властивості, іонна агрегація*

LUMINESCENCE AND SCINTILLATION PROPERTIES OF Cs_3ZnCl_5 AND $Cs_3ZnCl_5(Eu)$ SINGLE CRYSTALS

O. Yurchenko[*,a], O. Rebrov[†,b], V. Cherginets[†,c], I. Boyarintseva[†,d], T. Rebrova[†,e], T. Ponomarenko[†,f], O. Lebedinskiy[‡,g], O. Zelenskaya[†,h]

[*]*V.N. Karazin Kharkiv National University, School of Chemistry, 4 Svobody sqr.,61022, Kharkiv, Ukraine*
[†]*Institute for scintillation materials of National Academy of Sciences of Ukraine, 60 Nauky Avenue,61072, Kharkiv, Ukraine*
[‡] *SSI "Institute for Single Crystals" of NAS of Ukraine, 60, Nauky ave., Kharkiv, 61072, Ukraine*

a) yurchenko@karazin.ua   https://orcid.org/0000-0002-7117-4556
b) alrebrov@outlook.com   https://orcid.org/0000-0002-3105-8550
c) v_cherginets@ukr.net   https://orcid.org/0000-0002-2308-8979
d) gnyavamibigot@gmail.com   https://orcid.org/0000-0002-5219-6127
e) tp_rebrova@ukr.net   https://orcid.org/0000-0002-0077-3252
f) tv_ponomarenko@meta.ua   https://orcid.org/0000-0003-1809-3877
g) alexey.lebedinsky@gmail.com   https://orcid.org/0000-0003-2020-9939
h) olga.isma@gmail.com   https://orcid.org/0000-0001-7690-1110

This paper reports the results on obtaining and investigation of functional parameters of Cs_3ZnCl_5 crystals grown using Bridgman method from the melts of $3CsCl-2ZnCl_2$ and $3CsCl-1.995ZnCl_2-0.005\ EuCl_2$ compositions. The study of photoluminescence spectra obtained at 237 nm excitation shows the presence of the following emission bands: one at 325 nm caused by the defects or impurities, slightly pronounced band at *ca*. 450 nm caused by the presence of Eu^{2+} ions and a series of bands in 590÷700 nm range due to the presence of Eu^{3+} in the crystals. The presence of said Eu ions is confirmed by the luminescent studies with the use of excitation at wavelengths proper to Eu^{2+} (340 nm) and Eu^{3+} (465 nm). X-ray luminescence spectra include the bands with maxima of 235 nm and 285 nm which are caused by the core-valence luminescence, the band with the maximum at 320 nm caused by the defects and impurities and two bands with the maxima at 400 and 520 nm which nature is not clear (probably, it can be connected with the presence of Eu^{3+} in the samples). The study of light yield performed at the light collection time of 2 µs showed that for all the samples its value is *ca*. 6% vs. BGO crystal ($Bi_4Ge_3O_{12}$) and the form of the pulse-height spectra for the crystals grown from both melts practically coincide. This leads to the conclusion that the transfer of excitation from the matrix to Eu^{2+} ions is absent and, according to the photoluminescence studies it can be assumed that Eu^{2+} exists in the said crystals as inclusions of $CsCl:Eu^{2+}$ solid solution.

***Keywords:** cesium chloride, zinc chloride, europium chloride, luminescence, scintillation, light yield.*

Introduction

The recent progress of material science of halide scintillation materials is connected with the development of rare-earth activated (Eu^{2+}, Ce^{3+}) simple and complex compounds and their solid solutions. Some of the recently discovered materials are already established trademarks ($LaCl_3:Ce^{3+}$ – BrilLanCe^{TM}350 [1, 2] and $LaBr_3:Ce^{3+}$ – BrilLanCe^{TM}380 [2, 3]) and others ($SrI_2:Eu^{2+}$ [4] and $Cs_2LiYCl_6:Ce^{3+}$ (CLYC) [5]) are efficiently developed and also are commercially available [6,7]. The said materials are solid solutions of halides formed by perfectly isomorphic cations, e.g., $LaCl_3:Ce^{3+}$ means $La_{1-x}Ce_xCl_3$ and so on.

The search for new activated halide luminescent materials is performed among solid solutions formed by restrictedly isomorphic cations, e.g., for Eu^{2+}-activated materials compounds formed by Ca^{2+} [8] and Mg^{2+} [9] have been investigated.

This work presents an attempt to obtain Eu^{2+}-activated material on the basis of Cs_3ZnCl_5 compound formed by Zn^{2+} cation restrictedly isomorphic to Eu^{2+}. According to [10] the difference of the

electronegativities of Eu and Zn is 0.4 that is the limiting value for the perfect isomorphism (The Goldschmidt rule), as for the difference of the ionic radii [11] it considerably exceeds 15%.

It should be noted that the said non-activated material is also referred to scintillators for detection of X-ray irradiation [12].

The results of our study are presented below.

Experimental part

Reagents. Extra pure cesium chloride was used for the crystal growth of crystals on the basis of Cs_3ZnCl_5.

Zinc chloride was obtained by the dissolution of metallic zinc of reagent grade in extra pure hydrochloric acid according to well-known routine [13]. Obtained $ZnCl_2$ was grinded in glow box and kept there.

Charge for the growth of Cs_3ZnCl_5 was prepared by mixing of CsCl with $ZnCl_2$ in glow box in the mass ratio of 3,71:1.

The charge for the preparation of the growth melt of Cs_3ZnCl_5 melt with addition of 0.5 mol. % of Eu^{2+} with respect to Zn^{2+} was prepared in such a manner. Primarily solid solution of $CsCl-EuCl_2$ composition was prepared by the dissolution of 0.0882 g of Eu_2O_3 in 50 g of molten CsCl by the carbohalogenation process at 700 °C:

$$2\,Eu_2O_3 \downarrow +3\,CCl_4 = 4\,EuCl_2 + 3\,CO_2 \uparrow +2\,Cl_2 \uparrow \qquad (1)$$
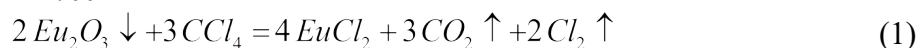
The primarily formed suspension of Eu_2O_3 disappeared after 1h treatment the melt became transparent and further it was treated for 1 h, cooled, grinded and kept in glow box. The temperature of the carbohalogenation provided practically complete reduction of $EuCl_3$ into $EuCl_2$.

For the preparation of Cs_3ZnCl_5:0.5 mol. % of Eu^{2+} charge 19.72 g of $CsCl:Eu^{2+}$ powder was mixed in the glow box with 5.282 g of $ZnCl_2$.

The growth procedure. The charge was placed in quartz ampoule of 12 mm diameter and 500 mm height. Before the growth the ampoule with the charge was kept under vacuum (1 Pa) for 24 h at 700 °C.

The growth of the crystals was performed by Bridgman method in two-zone furnace, the difference of temperature between the zones was 80 °C, temperature gradient was ca. 40 °C/cm, the rate of the dropping of the ampoule was 3.2 mm/h. After the finishing of the ampoule broaching the furnace was cooled to room temperature during 72 h.

After the cooling, ampoule was placed in the glow box where it was broken down and the ingot was removed. The transparent part of the ingot was cut, polished and kept in polyethylene batch in the glow box. The samples presented cylinders of 6÷10 mm diameter and 1 mm height.

The obtained samples were practically non-hygroscopic, therefore, they were not packed into containers at all the investigations.

Investigation of the obtained samples. The phase composition of the parts of the obtained ingot was determined using X-ray diffractometer DRON with Cu-Kα radiation.

The study of luminescent properties of the obtained samples was performed using a combined fluorescent lifetime and steady-state spectrometer FLS 920 (Edinburgh Instruments) equipped with a xenon Xe 450 W and hydrogen filled nF 900 nanosecond flashlamp for time correlated single photon counting measurements. Photoluminescence excitation (PLE) spectra were corrected on the incident photon flux. Photoluminescence emission (PL) spectra were corrected for the spectral sensitivity of the detection system.

The spectra of X-ray excited luminescence were obtained under X-ray (Cu, 40 kV, 40 μA) excitation in transmission mode and were not corrected for the spectral sensitivity of the detection system.

Scintillation decay time profiles of Cs_3ZnCl_5-based samples were obtained as follows. The samples were placed on the photocathode of Hamamatsu R6231 PMT. Scintillations were excited with 662 keV gammas from ^{137}Cs source. Signal from PMT anode was fed to the input of Rigol DS6064 oscilloscope. Decay curves were calculated by averaging of several hundreds of recorded pulses with amplitudes approximately corresponding to the full absorption peak.

The light yield and the energy resolution of the obtained samples were determined by the method of comparison [14]. The measurements were recorded using a pulse processing chain consisting of an

R1307 SU 0192 PMT (Hamamatsu, Japan), a charge-sensitive preamplifier BUS 2-95, a custom shaping amplifier and a multichannel analyzer AMA-03F. Relative light yield was determined by comparing the peak position (abscissa) of the grown crystals and that of a BGO ($Bi_4Ge_3O_{12}$) crystal (10,000 photons/MeV and energy resolution of 10 %). All measurements were done under the same conditions using the shaping time of 8 μs. The error of the light yield and energy resolution measurements was less than 5 %.

Results and discussion

As it was mentioned in the previous section all the ingots consisted of lower opaque part and upper transparent one. Taking into account that Eu^{2+} is slightly isomorphic to Zn^{2+} we performed examination of both parts of the ingot. The X-ray diffraction patterns of the said samples coincide.

The X-ray diffraction pattern of the samples grown from Cs_3ZnCl_5 melt containing $EuCl_2$ is presented in Fig. 1. It is seen that the ingots consist of Cs_3ZnCl_5 (tetragonal unit cell, a=0.926 nm, c=1.450 nm, space group I4/mcm) [15].
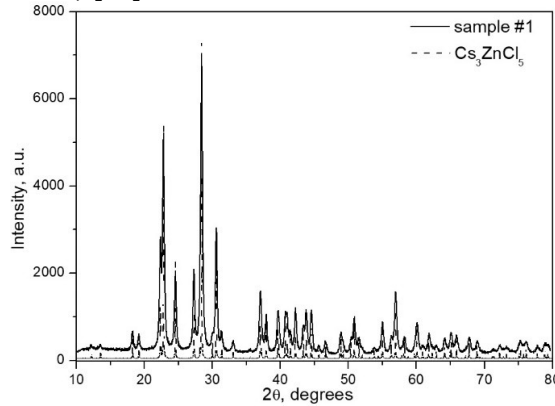
Figure 1. The X-ray diffraction pattern of the sample grown from Cs_3ZnCl_5 (Eu) melt (thick line) and the database data for Cs_3ZnCl_5 (thin line)

It means that there was no selective accumulation in the opaque part of CsCl or its compounds with $EuCl_2$ of $CsEuCl_3$ composition (tetragonal unit cell, a=0.5588(4) nm, c=0.5619(8) nm, space group P4 mm) [16]. It may be concluded that Eu^{2+} is distributed throughout all the ingot.

The excitation and photoluminescence spectra of the transparent part of the sample are presented in Fig. 2.
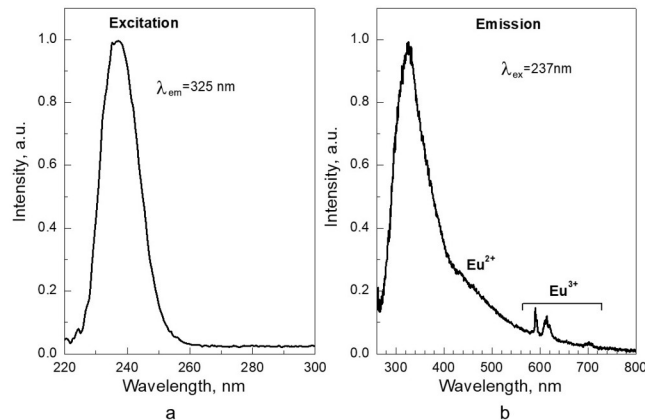
Figure 2. Excitation (a, λ_{em}=325 nm) and emission (b, λ_{ex}=237 nm) spectra of sample grown from Cs_3ZnCl_5 (Eu) melt

It can be seen that the main luminescence band at excitation wavelength of 237 nm is placed at 310 nm. Authors [12] found that similar band with the emission band 290 nm was obtained under excitation at 70÷90 nm and it was ascribed to Auger-free luminescence (AFL). In [17] the same authors studied luminescence of crystals of $Cs(Ca_{1-x}Mg_x)Cl_3$ composition and found that at the excitation at 240 nm the luminescence for all the studied materials is observed in 350÷390 nm range. Taking into account the excitation wavelength (240 nm) the authors assumed that this luminescence is

caused by defects or impurity sites. It is very probable that the emission band at 310 nm is also due to impurities or defects. The decay profile for the luminesce excited at 237 nm is monoexponential and the decay constant is estimated as 260 ns.

The beside of the above-discussed band in the emission spectra there is also the band proper to Eu^{2+} (~430 nm, slightly pronounced) and Eu^{3+} (three bands in 590÷700 nm region).

To check whether the 430 nm band is caused by the presence of Eu^{2+} we recorded the photoluminescence spectra using excitation at 340 nm proper for Eu^{2+}. These spectra are shown in Fig. 3.
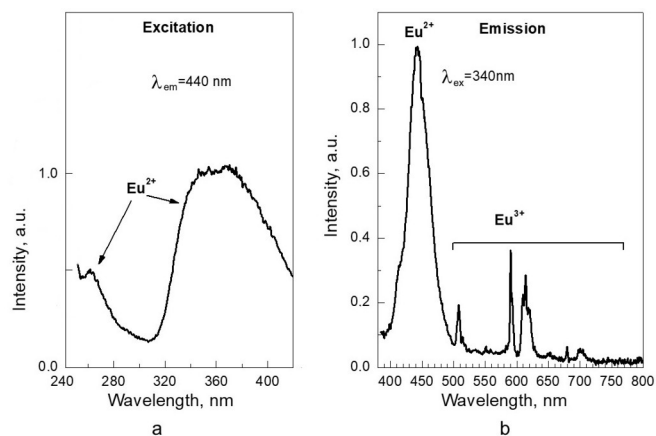
Figure 3. Excitation (a, λ_{em}=440 nm) and emission (b, λ_{ex}=340 nm) spectra of sample grown from Cs_3ZnCl_5 (Eu) melt

The excitation spectrum includes bands at 260 nm and wide band at 330÷400 nm that is proper to excitation of Eu^{2+} ions and the emission band at 442 nm. We can assume that the 442 nm band can be ascribed to the formation of $CsCl:Eu^{2+}$ solid solution since the same wavelength was obtained by the authors of [18].

As for the luminescence decay curve, it is presented in Fig. 4 and can be described by three components with decay constants of 17, 68 and 360 ns.
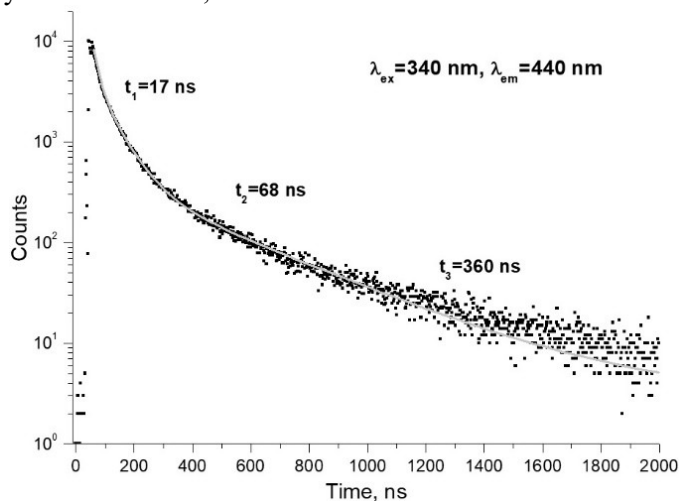
Figure 4. The decay curve (λ_{ex}=340 nm, λ_{em}=440 nm) for the sample grown from Cs_3ZnCl_5 (Eu) melt

It is interesting that authors [18] estimated the decay constant of longer component as 360 nm.

As for the presence in the sample of Eu^{3+}, it is easily confirmed by the data of Fig. 5.
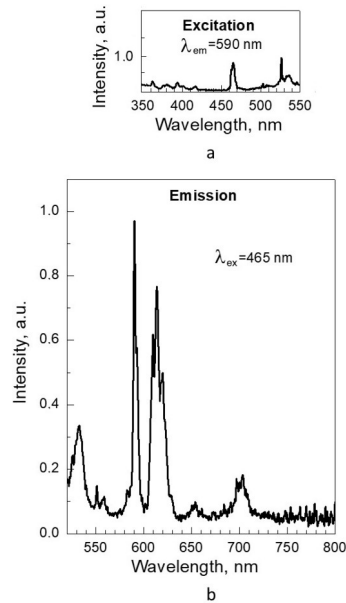
Figure 5. Excitation (a, λ_{em}=590 nm) and emission (b, λ_{ex}=465 nm) spectra of sample grown from Cs_3ZnCl_5 (Eu) melt

The emission spectrum includes bands at 590, 612 and 700 nm which are referred to luminescence of Eu^{3+}. So, at least the traces of $EuCl_3$ are present in the sample. This is proper to other chloride materials doped with Eu^{2+} since the decomposition temperature of $EuCl_3$ to $EuCl_2$ is close to 700 °C and even long-term keeping of the growth melt under vacuum does not provide the complete decomposition of $EuCl_3$ to $EuCl_2$.

Now let us consider results connected with the scintillation properties of the obtained crystals. The X-ray luminescence spectrum is presented in Fig. 6.

According to [12] the bands with maxima of 235 nm and 285 nm can be referred to core-valence luminescence, the band with the maximum at 320 nm according to the description of Fig. 1 is caused by the defects and impurities. As for the band with the maximum at 520 nm its nature is unknown, it may be caused by the presence of Eu^{3+} in the samples.
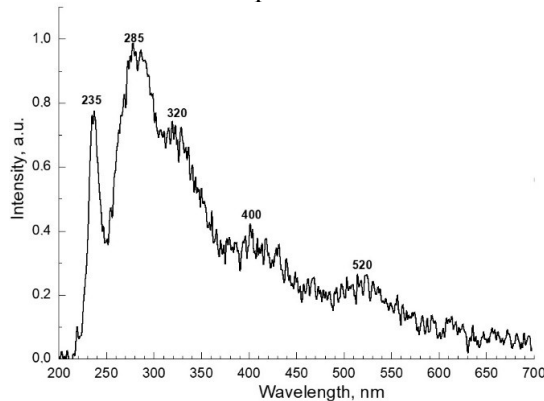
Figure 6. X-ray luminescence spectrum of sample grown from Cs_3ZnCl_5 (Eu) melt (reflectance mode, silver anode, I=40 μA, U=40 kV)

As for the light yield and energy resolution the light collection time of 2 μs was chosen going from the luminescence decay constants, the pulse-height spectra of the obtained crystals are presented in Fig. 7.

From Fig. 7a it follows that the light yield of Cs_3ZnCl_5(Eu) is equal to 5.8 % against BGO, i.e., *ca.* 580 photons per MeV. As for undoped Cs_3ZnCl_5 its light yield achieves 6 % against BGO (600 photons MeV), that agrees with the data of [12]. Due to complex structure of the photopeaks of the obtained crystals (Fig. 7b) any estimations of the energy resolution would be incorrect.

So, the light yield of Cs_3ZnCl_5 is not dependent on the presence or absence of Eu^{2+} ions in the sample and the pulse-height spectra are identical (Fig.7b). It means that the transfer of the excitation from matrix to Eu^{2+} ion is negligible or absent due to restricted isomorphism of Eu^{2+} and Zn^{2+} ions, which is confirmed by the data of Fig. 6. The most possible form of Eu^{2+} existence in the grown crystals considered in this paper may be $CsCl:Eu^{2+}$ inclusions or traces of $CsEuCl_3$ (see Fig. 3 and description for it).
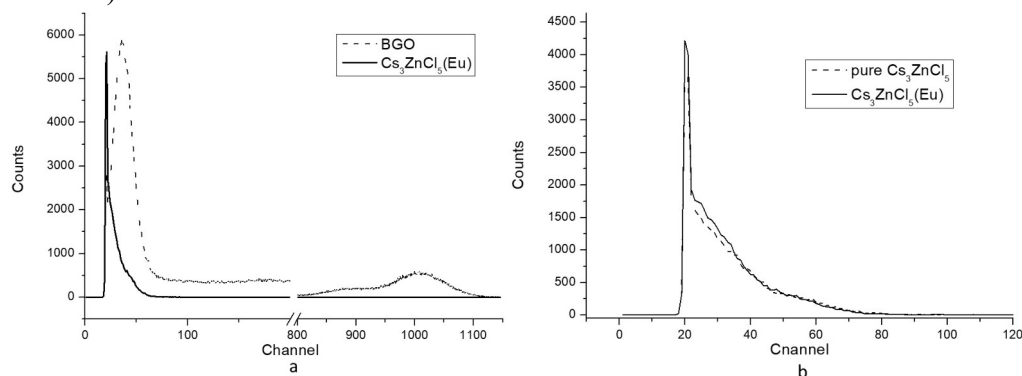
Figure 7. Pulse height spectra of: 1 – Cs_3ZnCl_5:(Eu) sample vs. BGO ($Bi_4Ge_3O_{12}$, standard), 2 – a comparison of the spectra for undoped Cs_3ZnCl_5 and Cs_3ZnCl_5 :(Eu)

Conclusions

In this study crystals on the basis of Cs_3ZnCl_5 were grown by Bridgman method from the melts of $3CsCl-2ZnCl_2$ and $3CsCl-1.995ZnCl_2-0.005\ EuCl_2$ compositions.

The luminescence spectra of the Cs_3ZnCl_5 samples obtained at λ_{ex}=237 nm include bands caused by defects or admixtures (325 nm), Eu^{2+} ions (450 nm) and Eu^{3+} ions (in the range of 590÷700 nm). The presence of both Eu ions was confirmed by luminescence investigations at excitation at wavelengths proper for the corresponding ions. The X-ray luminescence spectra did not include the bands proper for Eu ions.

The study of light yield performed at the light collection time of 2 μs showed that the light yield of the crystals grown from both melts is ca. 6% *vs*. BGO ($Bi_4Ge_3O_{12}$) and the shapes of the pulse-height spectra are practically the same that confirms the negligible excitation transfer from the matrix to Eu^{2+} ions. Taking into account the results of photoluminescence studies it can be assumed that Eu^{2+} ions exist in the grown Cs_3ZnCl_5 crystals as inclusions of $CsCl:Eu^{2+}$ solid solution.

References

1. Shah, K.S.; Glodo, J.; Klugerman, M.; Cirignano, L.; Moses, W.W.; Derenzo, S.E.; Weber, M.J.. $LaCl_3$:Ce Scintillator for Gamma Ray Detection. *Nucl. Instr. Meth. Prys.Res. A*. **2003**, *505*(1-2), 76-81. https://doi.org/10.1016/S0168-9002(03)01024-6.
2. https://www.gammadata.se/assets/Uploads/SGC-BrilLanCe-Scintillators-Performance-Summary2.pdf (Last visited February 9 2024).
3. Van Loef, E.V.D.; Dorenbos, P.; van Eijk, C.W.E.; Krämer, K.W.; Güdel, H.U. Scintillation properties of $LaBr_3$:Ce^{3+} crystals: fast, efficient and high-energy-resolution scintillators. *Nucl. Instr. Meth. Prys.Res. A*. **2002**, *486*, 254-258. https://doi.org/10.1016/S0168-9002(02)00712-X.
4. Cherepy, N.J.; Hull, G.; Drobshoff, A.D.; Payne, S.A.; van Loef, E.; Wilson, C.M.; Shah, K.S., Roy, U.N.; Burger, A.; Boatner, L.A.; Choong, W.-S.; Moses, W.W. Strontium and barium iodide high light yield scintillators. *Appl.Phys.Lett*. **2008**, *92*, 083508. https://doi.org/10.1063/1.2885728.
5. Bessière, A.; Dorenbos, P.; van Eijk, C.W.E.; Krämer, K.W.; Güdel H.U. Luminescence and scintillation properties of Cs_2LiYCl_6:Ce^{3+} for gamma and neutron detection. *Nucl. Instr. Meth. Prys.Res. A*. **2004**, *A 537*, 242 – 246. https://doi.org/10.1016/j.nima.2004.08.018.
6. https://www.advatech-uk.co.uk/sri2_eu.html (Last visited February 9 2024).
7. https://www.advatech-uk.co.uk/clyc_ce.html (Last visited February 9 2024).
8. Zhuravleva, M.; Blalock, B.; Yang, K.; Koschan, M.; Melcher C.L. New single crystal scintillators: $CsCaCl_3$:Eu and $CsCaI_3$:Eu. *J. Cryst. Growth*. **2012**, *352*(1).-P.115-119. https://doi.org/10.1016/j.jcrysgro.2012.02.025.

9. Suta, M.; Lavoie-Cardinal, F.; Olchowka, J.; Wickleder, K. Nature of localized excitons in CsMgX$_3$ (X=Cl, Br, I) and their interactions with Eu^{2+} ions. *Phys. Rev. Appl.* **2018**, *9*, 064024. https://doi.org/10.1103/PhysRevApplied.9.064024.
10. https://sciencenotes.org/list-of-electronegativity-values-of-the-elements/ (Last visited February 9 2024).
11. http://abulafia.mt.ic.ac.uk/shannon/radius.php (Last visited February 9 2024).
12. Takahashi, K; Arai, M.; Koshimizu, M.; Fujimoto, Y.; Yanagida, T.; Asai, K. Luminescence and scintillation properties of Cs$_2$ZnCl$_4$ and Cs$_3$ZnCl$_5$. *Jap. J. Appl. Phys.* **2020**, *59*, 072002. https://doi.org/10.35848/1347-4065/ab9655.
13. Karyakin, Yu,V.; Angelov, I.I. Pure chemical substances. 4th ed. *Khimiya*: Moscow, 1974, [In Russian]. https://libarch.nmu.org.ua/handle/GenofondUA/4615.
14. Sysoeva, E.; Tarasov, V.; Zelenskaya, O. Comparison of the methods for determination of scintillation light yield. *Nucl. Instr. Meth. Prys.Res. A*. **2002**. *486*(1-2), 67-73. https://doi.org/10.1016/S0168-9002(02)00676-9.
15. https://next-gen.materialsproject.org/materials/mp-570262/ (Last visited February 12 2024)
16. Nocera, D.G.; Morss, L.R.; Fahey J.A. Preparation, crystal structure, and enthalpy of formation of cesium europium(II) chloride, CsEuCl$_3$. *J. Inorg. Nucl. Chem*. **1980**, *42*(1), 55-59. https://doi.org/10.1016/0022-1902(80)80043-1.
17. Takahashi, K; Arai, M.; Koshimizu, M.; Fujimoto, Y.; Yanagida, T.; Asai, K. Auger-free luminescence characteristics of Cs(Ca$_{1-x}$Mg$_x$)Cl$_3$. *Nucl. Instr. Meth. Prys.Res. A*. **2020**, *954*, 161842. https://doi.org/10.1016/j.nima.2019.01.068.
18. Saeki, K.; Koshimizu, M.; Fujimoto, Y.; Yanagida, T.; Okada, G.; Yahaba, T.; Tanaka, H.; Asai K. Scintillation properties of Eu-doped CsCl and CsBr crystals. Opt. Mater. **2016**, 61, 125-128. https://doi.org/10.1016/j.optmat.2016.07.040.

О. І. Юрченко*, О. Л. Ребров†, В. Л. Чергинець†, Я. А. Бояринцева†, Т. П. Реброва†, Т. В. Пономаренко†, О. М. Лебединський‡, О. В. Зеленська†. Люмінесцентні і сцинтиляційні властивості монокристалів кристалів Cs$_3$ZnCl$_5$ та Cs$_3$ZnCl$_5$(Eu).

*Харківський Національний університет ім. В.Н. Каразіна, хімічний факультет, пл. Свободи, 4, 61022, Харків, Україна
†Інститут сцинтиляційних матеріалів Національної академії наук України, пр. Науки, 60, 61072, Харків, Україна
‡НТК "Інститут монокристалів" Національної академії наук України, пр. Науки, 60, 61072, Харків, Україна

Наведено результати робіт з отримання і дослідження функціональних властивостей кристалів Cs$_3$ZnCl$_5$, вирощених з розплавів складів 3CsCl-2ZnCl$_2$ і 3CsCl-1.995ZnCl$_2$-0.005 EuCl$_2$. У спектрах фотолюмінесценції кристалів, одержаних при λ$_{em}$=237 нм, спостерігається смуга з максимумом при 325 нм, яка може бути обумовлена наявністю дефектів і домішок, слабка смуга при ~450 нм, що відноситься до люмінесценції Eu^{2+}, а також серія смуг в інтервалі 590-700 нм, які відносяться до люмінесценції Eu^{3+}. Присутність іонів європію Eu було доведено дослідженнями люмінесценції при збудженні на довжинах хвиль притаманних для Eu^{2+} (340 нм) і Eu^{3+} (465 нм). Спектри рентгенолюмінесценції містять смуги з максимумами при 235 нм і 285 нм, що відповідають остовно-валентній люмінесценції, при 320 нм (можливо, дефекти і домішки) і дві смуги з максимумами при 400 і 520 нм, природа яких не з'ясована (можливо, вони пов'язані з присутністю іонів Eu^{3+} у зразках). Дослідження світлового виходу одержаних кристалів, проведені при часі світлозбирання 2 мкс, показали, що кристали обох складів мають світловихід приблизно 6% відносно кристалів BGO (Bi$_4$Ge$_3$O$_{12}$), а форма їх амплітудних спектрів практично однакова, що свідчить про незначний перенос збудження від матриці до іонів Eu^{2+}. Виходячи з результатів дослідження фотолюмінесценції, можна припустити, що Eu^{2+} існує у вирощених кристалах у вигляді включень твердого розчину CsCl:Eu^{2+}.

Ключові слова: *хлорид цезію, хлорид цинку, хлорид європію, люмінесценція, сцинтиляційні властивості, світловий вихід.*

ANALYSIS OF VOLUMETRIC PROPERTIES OF LIQUID MIXTURES
I. METHOD OF BINARY ADDITIVE QUASI-SOLVATES

P.V. Efimov

V. N. Karazin Kharkiv National University, School of Chemistry, 4 Svobody sqr., Kharkiv, 61022 Ukraine

✉ pavel.v.efimov@karazin.ua   https://orcid.org/0000-0003-1781-3844

The method of binary additive quasi-solvates (BAQS) a new approach for analyzing the physicochemical properties of solutions is proposed. Quasi-solvate Q_{ij} is a hypothetical two-particle structure in which one particle i is the 'solute' and the other particle j is the 'solvent'. A set of similar quasi-solvates has the macroscopic property F_{ij}. The solution is an additive mixture of quasi-solvates with weight functions w_{ij}. Two models have been developed within the BAQS method: with symmetric weight functions (BAQS/S) and with asymmetric weight functions (BAQS/A). On the example of volumetric properties of non-electrolyte solutions the possibilities of the method are shown. Effective limiting partial molar volumes of components for mixtures of non-electrolytes are determined. The possibility of predicting the properties of multicomponent solutions from data for two-component systems is considered. Applications to other solution properties are shown. Each of the proposed models has its own advantages and limitations.

BAQS/S: describes molar volumes of mixtures, especially for aprotonic systems, can be used to predict properties of multicomponent systems, effective on small datasets. Limitations: applicability to other solution properties remains questionable, model parameters differ from those obtained by the independent method, approximation accuracy is inferior to empirical models.

BAQS/A: applicable for any solution properties, informative and illustrative. Limitations: very sensitive to the choice of approximating equation, difficult to interpret results, developed only for two-component systems.

Keywords: *physicochemical analysis, molar volume, limiting partial molar volume, Redlich-Kister equation, non-electrolyte solutions, multicomponent mixtures, binary additive quasi-solvates.*

Introduction

Solutions play a significant role in all areas of chemistry. One of the most important thermodynamic characteristics of solutions are volumetric properties: density, molar volume, excess molar volume[1]. A great number of data on volumetric properties of solutions have been collected[2] and they continue to be actively studied[3-6]. The properties of solutions are determined by the specifics of interparticle interactions. Therefore, analyzing the influence of the composition and nature of components on the physicochemical properties of solutions is an actual problem. In many cases, this requires special experiments. Which significantly limits the range of systems to be investigated.

Volumetric properties are usually considered in terms of molar volumes. For example, analysis of the dependence of molar volume on composition for two-component solutions. Excess molar volume is a measure of the deviation of molar volume from additivity:

$$V^E = V - V_1 x_1 - V_2 x_2 \tag{1}$$

Traditionally, the dependence of excess molar volume on composition is described by the empirical Redlich-Kister equation[7]:

$$V^E = x_1 x_2 \left(A_0 + \sum_{i=1}^{n} A_i (x_1 - x_2)^i \right) \tag{2}$$

Each system is characterized by a set of empirical parameters A_i.

Another approach is the partial molar volume method:

$$V = \overline{V_1} x_1 + \overline{V_2} x_2 \tag{3}$$

Of particular interest are the limiting partial molar volumes. Within the framework of the Redlich-Kister model, limiting partial molar volumes are determined:

$$\overline{V}_{12}^{\infty} = V_1 + \sum_{i=0}^{n} A_i \cdot (-1)^i \tag{4}$$

$$\overline{V}{}^{\infty}_{21} = V_2 + \sum_{i=0}^{n} A_i \tag{5}$$

A large amount of data in the dilute region of compositions is needed to correctly determine the limiting partial molar volumes. At the same time, most non-electrolyte solutions have been studied with a typical composition scale step of ~0.1 mole fraction units, which is only a dozen points for each system. Thus, using equation (2) with a large number of parameters seems incorrect. Despite the colossal number of systems studied (about a hundred thousand datasets, more than a million experimental points[2]), the vast majority of data more than to determine the excess molar volume is not used in any way.

This paper proposes a method to analyze the physicochemical properties of solutions within a single dataset. This will allow the extensive material collected in the scientific literature to be utilized.

Method

Binary Additive Quasi-Solvates (BAQS).

Let's introduce some definitions.

D1: Quasi-solvate Q_{ij} is a hypothetical two-particle structure in which one particle i is the 'solute' and the other particle j is the 'solvent'.

D2: A set of similar quasi-solvates has the macroscopic property F_{ij}.

D3: The solution is an additive mixture of quasi-solvates with weight functions w_{ij}.

From *D2* and *D3*, it follows that the property F of an n-component solution is composed of F_{ij} with weight functions w_{ij}:

$$F = \sum_{i=1}^{n} \sum_{j=1}^{n} F_{ij} w_{ij} \tag{6}$$

$$\sum_{i=1}^{n} \sum_{j=1}^{n} w_{ij} = 1 \tag{7}$$

Four types of quasi-solvates are possible for a two-component solution:

Q_{11} – component 1 particle is the 'solute', component 1 particle is the 'solvent';

Q_{22} – component 2 particle is the 'solute', component 2 particle is the 'solvent';

Q_{12} – component 1 particle is the 'solute', component 2 particle is the 'solvent';

Q_{21} – component 2 particle is the 'solute', component 1 particle is the 'solvent'.

Thus, the molar volume of the two-component solution is

$$V = V_{11} w_{11} + V_{12} w_{12} + V_{21} w_{21} + V_{22} w_{22} \tag{8}$$

Cases V_{11} and V_{22} – correspond to pure components. Based on *D1*, it can be assumed that

$$V_{12} = \frac{\overline{V}{}^{\infty}_{12} + V_{11}}{2} \text{ and } V_{21} = \frac{\overline{V}{}^{\infty}_{21} + V_{22}}{2} \tag{9}$$

It remains only to set the weight functions. Two approaches to solving this problem are proposed.

Binary Additive Quasi-Solvates with Symmetric weight functions (BAQS/S)

Let the quasi-solvates be randomly distributed in the solution. Then the weight function is equal to the probability of choosing two particles:

$$w_{11} = x_1^2 \text{ and } w_{22} = x_2^2 \tag{10}$$

$$w_{12} + w_{21} = 2 x_1 x_2 \tag{11}$$

On the other hand, by definition

$$\overline{V}{}^{\infty}_{12} = V_{22} - \frac{\partial V}{\partial x_1}\Big|_{x_1=0} \text{ and } \overline{V}{}^{\infty}_{21} = V_{11} - \frac{\partial V}{\partial x_2}\Big|_{x_2=0} \tag{12}$$

Conditions (8-12) satisfy the formulas:

$$w_{12} = 2 x_1 x_2^2 \text{ and } w_{21} = 2 x_1^2 x_2 \tag{13}$$

This suggests that the distribution of the quasi-solvates Q_{12} and Q_{21} cannot be completely random, but depends on the environment. Conditions (10, 13) satisfy the formula:

$$w_{ij} = \frac{2x_i x_j^2}{x_i + x_j} \tag{14}$$

Thus, the weight functions are symmetric with respect to substitution of indices.

From (8-10, 13) it follows that

$$V = V_{11}x_1^2\left(1 + x_2\right) + \overline{V}_{12}^\infty x_1 x_2^2 + \overline{V}_{21}^\infty x_1^2 x_2 + V_{22}x_2^2\left(1 + x_1\right) \tag{15}$$

The values of the molar volumes of pure components are assumed to be known. The limiting molar partial volumes are unknown and are calculated as fitting parameters. A special deviation function is used for approximation:

$$\Delta V = V - V_{11}x_1^2\left(1 + x_2\right) - V_{22}x_2^2\left(1 + x_1\right) = \overline{V}_{12}^* x_1 x_2^2 + \overline{V}_{21}^* x_1^2 x_2 \tag{16}$$

Normalized deviation function assumes linear dependence and allows visual assessment of model adequacy:

$$\Delta V_N = \frac{\Delta V}{x_1 x_2} = \overline{V}_{12}^* x_2 + \overline{V}_{21}^* x_1 \tag{17}$$

The coefficients of the two-parameter Redlich-Kister equation are related to the effective limiting partial molar volumes:

$$A_0 = \frac{\left(\overline{V}_{21}^* - V_{22}\right) + \left(\overline{V}_{12}^* - V_{11}\right)}{2} = \frac{V_{21}^{E*} + V_{12}^{E*}}{2} \tag{18}$$

$$A_1 = \frac{\left(\overline{V}_{21}^* - V_{22}\right) - \left(\overline{V}_{12}^* - V_{11}\right)}{2} = \frac{V_{21}^{E*} - V_{12}^{E*}}{2} \tag{19}$$

The BAQS/S model can also describe multi-component systems:

$$V = \sum_{i=1}^{n} \sum_{j=1}^{n} \left(\overline{V}_{ij}^\infty + V_{jj}\right) \frac{x_i x_j^2}{x_i + x_j} \tag{20}$$

The applicability of this model is discussed below.

Binary Additive Quasi-Solvates with Asymmetric weight functions (BAQS/A).

Assume that the equilibrium between quasi-solvates is established:

$$Q_{11} + Q_{22} \leftrightarrow Q_{12} + Q_{21} \tag{21}$$

$$Q_{12} \leftrightarrow Q_{21} \tag{22}$$

Then

$$w_{11} = x_1 - \alpha \tag{23}$$

$$w_{22} = x_2 - \alpha \tag{24}$$

$$w_{12} = \alpha - \beta \tag{25}$$

$$w_{21} = \alpha + \beta \tag{26}$$

where α and β are the mole fractions of the particles involved in processes (21) and (22), respectively.

From (3, 8, 9, 23-27) it follows that

$$V = V_{11}\left(x_1 - \frac{\alpha}{2} + \frac{\beta}{2}\right) + \overline{V}_{12}^\infty\left(\frac{\alpha}{2} - \frac{\beta}{2}\right) + \overline{V}_{21}^\infty\left(\frac{\alpha}{2} + \frac{\beta}{2}\right) + V_{22}\left(x_2 - \frac{\alpha}{2} - \frac{\beta}{2}\right) = \overline{V}_1 x_1 + \overline{V}_2 x_2 \tag{27}$$

Suppose it can be divided into two component parts:

$$V_{11}\left(x_1 - \frac{\alpha}{2} + \frac{\beta}{2}\right) + \overline{V}_{12}^\infty\left(\frac{\alpha}{2} - \frac{\beta}{2}\right) = \overline{V}_1 x_1 \tag{28}$$

$$V_{22}\left(x_2 - \frac{\alpha}{2} - \frac{\beta}{2}\right) + \overline{V}_{21}^\infty\left(\frac{\alpha}{2} + \frac{\beta}{2}\right) = \overline{V}_2 x_2 \tag{29}$$

After simple transformations the system of equations has the form:

$$\alpha - \beta = 2x_1 \frac{\overline{V}_1 - V_{11}}{\overline{V}_{12}^{\infty} - V_{11}} \tag{30}$$

$$\alpha + \beta = 2x_2 \frac{\overline{V}_2 - V_{22}}{\overline{V}_{21}^{\infty} - V_{22}} \tag{31}$$

From (23-26, 30, 31) it follows that

$$w_{12} = 2x_1 \frac{\overline{V}_1^E}{\overline{V}_{12}^{E\infty}} \text{ and } w_{21} = 2x_2 \frac{\overline{V}_2^E}{\overline{V}_{21}^{E\infty}} \tag{32}$$

$$w_{11} = x_1 - \frac{w_{12} + w_{21}}{2} \text{ and } w_{22} = x_2 - \frac{w_{12} + w_{21}}{2} \tag{33}$$

Thus, a set of weight functions of quasi-solvates for any composition of the system is obtained. The weight functions in model BAQS/A are asymmetric with respect to index substitution.

Let us determine the excess partial molar volumes using the tangent to the excess volume function (1). If we use (2), the weight functions are determined using the coefficients of the Redlich-Kister equation and special polynomials ($x \equiv x_2$):

$$w_{12} = 2(1-x) \frac{\sum\limits_{i=0}^{n} A_i P_{1i}}{\sum\limits_{i=1}^{n} A_i \cdot (-1)^i} \tag{34}$$

$$w_{21} = 2x \frac{\sum\limits_{i=0}^{n} A_i P_{2i}}{\sum\limits_{i=1}^{n} A_i} \tag{35}$$

The following are special polynomials:

$$P_{10} = x^2 \tag{36}$$
$$P_{11} = 3x^2 - 4x^3 \tag{37}$$
$$P_{12} = 5x^2 - 16x^3 + 12x^4 \tag{38}$$
$$P_{13} = 7x^2 - 36x^3 + 60x^4 - 32x^5 \tag{39}$$
$$P_{14} = 9x^2 - 64x^3 + 168x^4 - 192x^5 + 80x^6 \tag{40}$$
$$P_{15} = 11x^2 - 100x^3 + 360x^4 - 640x^5 + 560x^6 - 192x^7 \tag{41}$$
$$P_{16} = 13x^2 - 144x^3 + 660x^4 - 1600x^5 + 2160x^6 - 1536x^7 + 448x^8 \tag{42}$$
$$P_{20} = 1 - 2x + x^2 \tag{43}$$
$$P_{21} = 1 - 6x + 9x^2 - 4x^3 \tag{44}$$
$$P_{22} = 1 - 10x + 29x^2 - 32x^3 + 12x^4 \tag{45}$$
$$P_{23} = 1 - 14x + 61x^2 - 116x^3 + 100x^4 - 32x^5 \tag{46}$$
$$P_{24} = 1 - 18x + 105x^2 - 288x^3 + 408x^4 - 288x^5 + 80x^6 \tag{47}$$
$$P_{25} = 1 - 22x + 161x^2 - 580x^3 + 1160x^4 - 1312x^5 + 784x^6 - 192x^7 \tag{48}$$
$$P_{26} = 1 - 26x + 229x^2 - 1024x^3 + 2660x^4 - 4192x^5 + 3952x^6 - 2048x^7 + 448x^8 \tag{49}$$

For the two-parameter Redlich-Kister equation considering (18, 19), where ς is the ratio of the effective excess limiting partial molar volumes:

$$w_{11} = x_1^2 + 4x_1^2 x_2^2 \cdot \left(1 - \frac{\varsigma_{12} + \varsigma_{21}}{2}\right) \tag{50}$$

$$w_{22} = x_2^2 + 4x_1^2 x_2^2 \cdot \left(1 - \frac{\varsigma_{12} + \varsigma_{21}}{2}\right) \tag{51}$$

$$w_{12} = 2x_1 x_2^2 + 4x_1^2 x_2^2 \cdot (\varsigma_{21} - 1) \tag{52}$$

$$w_{21} = 2x_1^2 x_2 + 4x_1^2 x_2^2 \cdot (\varsigma_{12} - 1) \tag{53}$$

Restriction on the ratio of excess limiting partial molar volumes:

$$\frac{1}{2} \le \varsigma_{ij} \le 2 \tag{54}$$

When the excess limiting partial molar volumes are equal, the weight functions correspond to equations (10) and (13).

## Model testing

BAQS/S:Two-component systems.

Let us consider the applicability of the model for the well-studied Ethanol-Water system. Data on the density of water-alcohol mixtures at 298.15 K and atmospheric pressure are taken from [8]. Based on these data, the ΔV functions were calculated and approximated by equation (16). (Fig. 1). As fitting parameters, the limiting partial molar volumes of Ethanol in Water and Water in Ethanol were determined (Table 2, 2 parameters). The values obtained are slightly different from the traditional values 55.195 and 13.904 cm^3/mol, respectively [9]. Thus, the calculated limiting partial molar volumes should be considered as effective within the model.

The data are presented more clearly in the form of linearized equation (17). Figure 2 also shows the values for binary mixtures of Water, Acetonitrile and DMSO at 293.15 K and pressure of 81.5 kPa calculated from [10].
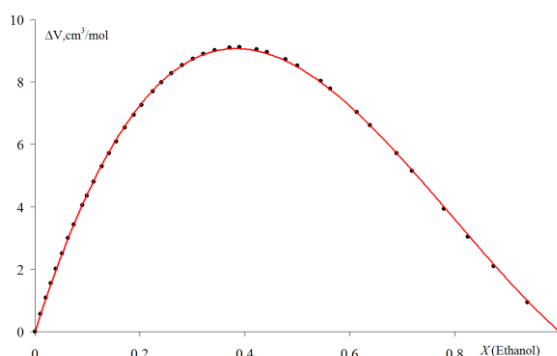
Fig. 1 Dependence of the function ΔV on the composition of the mixture of Water and Ethanol. The dots show experimental data, the line – calculation by equation (16).

It can be seen that the model describes the experimental data quite satisfactorily. Small deviations are observed for water-organic systems in the region of low water content.
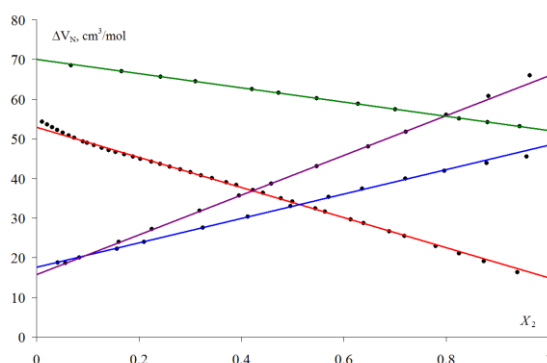
Fig. 2 Dependence of the function ΔV_N on the content of the second component of the mixture. Dots – experimental data. Lines – calculations according to equation (17): Ethanol-Water (red), Water-Acetonitrile (blue), Water-DMSO (purple), DMSO-Acetonitrile (green). See text for explanations.

However, it should be noted that BAQS/S is equivalent to the two-parameter Redlich-Kister equation and is inferior in accuracy to higher order equations. Nevertheless, it is reasonable to use it for small datasets and data visualization.

BAQS/S: Three-component systems.

The BAQS/S model can be used for multicomponent systems. The molar volumes of the three-component Water-Acetonitrile-DMSO system were calculated from the above data of the two-component systems and compared with experimental data [10]. Table 2 summarizes the parameters obtained for the two-component systems. Similar parameters determined only for three-component systems are also given.

Table 1. Effective limiting partial molar volumes V_{ij} (cm^3/mol) for two- and three-component systems.

i	j	2 components	3 components
Water	Acetonitrile	17.60±0.17	17.40±0.12
Acetonitrile	Water	48.43±0.17	48.82±0.11
Water	DMSO	15.77±0.16	15.63±0.11
DMSO	Water	65.90±0.16	65.91±0.11
Acetonitrile	DMSO	52.07±0.04	52.08±0.11
DMSO	Acetonitrile	70.08±0.04	68.97±0.12

The differences between the parameters obtained from different data are insignificant. The standard deviation for a three-component system is of the same order of magnitude as for two-component systems. Thus, the BAQS/S model can be applied to predict the properties of multicomponent systems.

BAQS/A: Molar volume.

The data of molar volumes of Water-Ethanol mixtures [8] were approximated by Redlich-Kister equations of different orders. The calculated parameters are summarized in Table 2.

Table 2. Parameters of equation (2), limiting partial molar volumes and sum of squares of deviations.

	2 parameters	3 parameters	4 parameters	5 parameters	6 parameters	7 parameters
A_0	-4.44±0.04	-4.29±0.03	-4.27±0.03	-4.20±0.02	-4.23±0.01	-4.26±0.01
A_1	1.29±0.09	1.10±0.06	1.34±0.10	1.16±0.08	0.77±0.06	0.88±0.03
A_2		-1.08±0.13	-1.23±0.13	-2.51±0.22	-2.01±0.13	-0.95±0.10
A_3			-0.74±0.26	-0.21±0.20	2.82±0.35	1.97±0.17
A_4				2.42±0.39	1.46±0.23	-3.23±0.40
A_5					-4.06±0.44	-2.91±0.22
A_6						4.81±0.40
$\overline{V}_{12}^{\infty}$	52.94±0.09	52.20	52.58	53.42	54.37	55.10
$\overline{V}_{21}^{\infty}$	14.92±0.11	13.80	13.17	14.72	12.82	14.38
σ	0.0574	0.0203	0.0166	0.0079	0.0023	0.0004

As the number of parameters increases, the approximation accuracy improves. However, the uncertainty of the limit values increases. Figures 3, 4, 5 show the dependences of weight functions for the two-, three-, and four-parameter Redlich-Kister equation calculated from equations (34, 35) and parameters of Table 3. Index 1 refers to Ethanol, index 2 to Water. The calculated weight functions depend significantly on the number of parameters of the approximating equation. Moreover, negative values of weight functions are observed for five and more parameters. However, qualitatively, the dependencies in Figs. 3-5 are similar. Thus, the question of choosing an approximating equation for the dependence of molar volume on composition remains open. Other approximating functions are also found in the literature[11]. For example, the Padé approximation or orthogonal Legendre polynomials are used.
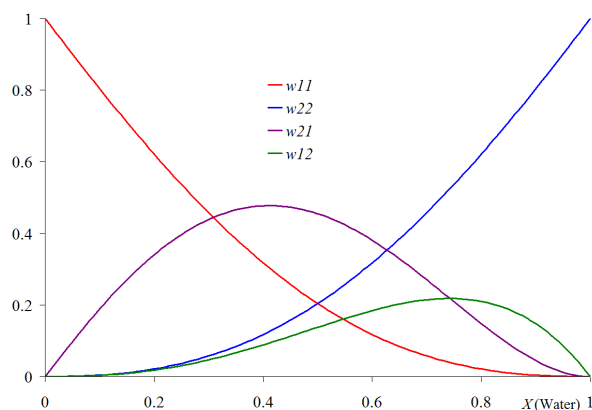
Figure 3. Dependence of weight functions on mixture composition for the two-parameter Redlich-Kister equation (see text for notations).
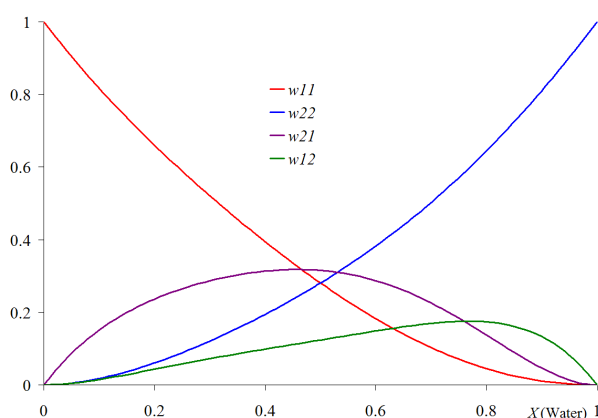
Figure 4. Dependence of weight functions on mixture composition for the three-parameter Redlich-Kister equation (see text for notations).
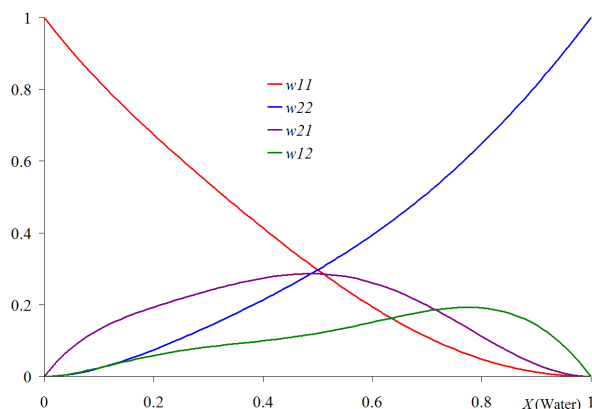
Figure 5. Dependence of weight functions on mixture composition for the four-parameter Redlich-Kister equation (see text for notations).

The difference in weight functions for BAQS/S and BAQS/A models characterizes the specificity of interparticle interactions:

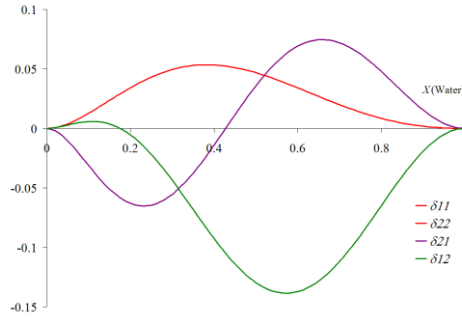$$\delta_{11} = w_{11} - x_1^2 \tag{55}$$

$$\delta_{22} = w_{22} - x_2^2 \tag{56}$$

$$\delta_{12} = w_{12} - 2x_1 x_2^2 \tag{57}$$

$$\delta_{21} = w_{21} - 2x_1^2 x_2 \tag{58}$$

what accounts for the deviations from linear dependence in equation 17.

Fig. 6 shows the differences of the weight functions for the four-parameter model.

Figure 6. Dependence of the weight function difference on the mixture composition (see text for explanations).

Weight function differences for a two-parameter model:

$$\delta_{11} = \delta_{22} = 4x_1^2 x_2^2 \cdot \left(1 - \frac{\varsigma_{12} + \varsigma_{21}}{2}\right) \tag{59}$$

$$\delta_{12} = 4x_1^2 x_2^2 \cdot (\varsigma_{21} - 1) \tag{60}$$

$$\delta_{21} = 4x_1^2 x_2^2 \cdot (\varsigma_{12} - 1) \tag{61}$$

Parameters δ_{ij} show which interactions between components predominate. However, the interpretation of the results obtained requires special caution. It should be remembered that we are not talking about real particles, but about hypothetical quasi-solvates, and the results obtained are only a method for describing the effects of interparticle interactions. The relationship of the BAQS method with other approaches remains to be studied.

BAQS/A. Molar heat capacity.

The BAQS/A model can also be used to analyze other properties of solutions. From the data [12] of molar heat capacity of Water-Ethanol solutions at 298.15K and atmospheric pressure, the parameters of the Redlich-Kister equation were calculated. Based on these parameters, weighting functions (32-35) and deviation parameters (55-58) are determined. Figure 7 shows the deviation functions calculated from the three-parameter Redlich-Kister model.
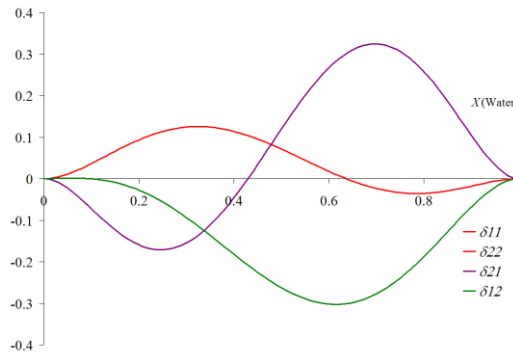
Figure 7. Dependence of the weight function difference on the mixture composition (see text for explanations).

Comparison with similar data for molar volumes (Fig. 6) shows that, despite the difference in the amplitude of deviations, general regularities in the distribution of weight functions of quasi-solvates are observed.

Conclusions

The method of binary additive quasisolvates is proposed. Two models considering in different aspects interparticle interactions in solutions are developed. Each of the proposed models has advantages and limitations.

BAQS/S: describes molar volumes of mixtures, especially for aprotonic systems, can be used to predict properties of multicomponent systems, effective on small datasets. Limitations: applicability to other solution properties remains questionable, model parameters differ from those obtained by the independent method, approximation accuracy is inferior to empirical models.

BAQS/A: applicable for any solution properties, informative and illustrative. Limitations: very sensitive to the choice of approximating equation, difficult to interpret results, developed only for two-component systems.

Nomenclature

ρ – solution density (g/cm^3);

ρ_i – density of i-th component (g/cm^3);

M_i – molar mass of i-th component (g/mol);

x_i – mole fraction of i-th component in solution;

x – mole fraction of the second component in the two-component solution ($x \equiv x_2$);

V_i – molar volume of pure i-th component (cm^3/mol)

$$V_i = \frac{M_i}{\rho_i};$$

V – molar volume of the n-component solution (cm^3/mol)

$$V = \frac{\sum_{i=1}^{n} M_i x_i}{\rho};$$

$\overline{V}_i$ – partial molar volume of i-th component in solution (cm^3/mol);

$\overline{V}_{ij}^{\infty}$ – limiting partial molar volume of solute i in solvent j (cm^3/mol);

$\overline{V}_{ij}^{*}$ – effective limiting partial molar volume of solute i in solvent j (cm^3/mol);

$\overline{V}_i^{E}$ – excess partial molar volume of i-th component in solution (cm^3/mol)

$$\overline{V}_i^{E} = \overline{V}_i - V_i;$$

$\overline{V}_{ij}^{E\infty}$ – excess limiting partial molar volume of solute i in solvent j (cm^3/mol)

$$\overline{V}_{ij}^{E\infty} = \overline{V}_{ij}^{\infty} - V_i;$$

$\overline{V}_{ij}^{E*}$ – effective excess limiting partial molar volume of solute i in solvent j (cm^3/mol)

$$\overline{V}_{ij}^{E*} = \overline{V}_{ij}^{*} - V_i;$$

ς_{ij} – ratio of the effective excess limiting partial molar volumes

$$\varsigma_{ij} = \frac{\overline{V}_{ij}^{E*}}{\overline{V}_{ji}^{E*}};$$

V_{ij} – molar volume of quasi-solvate Q_{ij} (cm^3/mol);

A_i – parameter of the Redlich-Kister equation (cm^3/mol);

ΔV – special deviation function (cm^3/mol);

ΔV_N – normalized special deviation function (cm^3/mol);

w_{ij} – weight function of the quasi-solvate Q_{ij};

δ_{ij} – difference of weight functions of the quasi-solvate Q_{ij};

References

1. Wilhelm E., Volumetric Properties: Introduction, Concepts and Selected Applications. In *Volume Properties: Liquids, Solutions and Vapours*, ed. E. Wilhelm and T. Letcher, The Royal Society of Chemistry, 2014, pp. 1-72. DOI:10.1039/9781782627043-00001

2. https://www.ddbst.com

3. Arnautovic Z., Kutzner S., Weith T., Heberle F., Brüggemann D. Density and Viscosity of Linear Siloxanes and Their Mixtures, *J. Chem. Eng. Data* **2023**, 68, 2, 314–329 DOI: 10.1021/acs.jced.2c00590

4. Kunstmann B., Kohns M., Hasse H. Thermophysical Properties of Mixtures of 2-Ethylhexanoic Acid and Ethanol, *J. Chem. Eng. Data* **2023**, 68, 2, 330–338 DOI: 10.1021/acs.jced.2c00689

5. Moodley K. Measurements of P-ρ-T for Propan-1-ol or Propan-2-ol + Oct-1-ene between 303.15–353.15 K and 0.1–20 MPa, *J. Chem. Eng. Data* **2023**, 68, 1, 25–39 DOI: 10.1021/acs.jced.2c00544

6. Hartono A., Knuutila H. K. Densities, Viscosities of Pure 1-(2-Hydroxyethyl) Pyrrolidine, 3-Amino-1-Propanol, Water, and Their Mixtures at 293.15 to 363.15 K and Atmospheric Pressure, *J. Chem. Eng. Data* **2023**, 68, 3, 525–535 DOI: 10.1021/acs.jced.2c00648

7. Redlich O., Kister A. T. Thermodynamics of Nonelectrolyte Solutions - x-y-t relations in a Binary System, *Ind. Eng. Chem.* **1948**, 40, 2, 341–345 DOI: 10.1021/ie50458a035

8. Hervello M. F., Sánchez A. Densities of Univalent Cation Sulfates in Ethanol + Water Solutions, *J. Chem. Eng. Data* **2007**, 52, 3, 752–756 DOI: 10.1021/je060335h

9. Marsh K.N., Richards A.E. Excess volumes for ethanol + water mixtures at 10-K intervals from 278.15 to 338.15 K, *Austral. J. Chem.* **1980**, 33, 10, 2121–2132 DOI:10.1071/CH9802121

10. Zarei H.A., Zare Lavasani M., Iloukhani H. Densities and Volumetric Properties of Binary and Ternary Liquid Mixtures of Water (1) + Acetonitrile (2) + Dimethyl Sulfoxide (3) at Temperatures from (293.15 to 333.15) K and at Ambient Pressure (81.5 kPa) *J. Chem. Eng. Data* **2008**, 53, 2, 578–585 DOI: 10.1021/je700645p

11. Wilhelm E., Grolier J.-P. E. Excess Volumes of Liquid Nonelectrolyte Mixtures. In *Volume Properties: Liquids, Solutions and Vapours*, ed. E. Wilhelm and T. Letcher, The Royal Society of Chemistry, **2014**, pp. 163-245. DOI: 10.1039/9781782627043-00163

12. Grolier J.-P.E., Wilhelm E. Excess volumes and excess heat capacities of water + ethanol at 298.15 K *Fluid Ph. Equilib.* **1981** 6, 3–4, 283–287. DOI: 10.1016/0378-3812(81)85011-X

П.В. Єфімов. Аналіз волюмометричних властивостей рідких сумішей. I. Метод бінарних адитивних квазісольватів

Харківський національний університет імені В. Н. Каразіна, майдан Свободи 4, Харків, 61022, Україна

Запропоновано новий підхід до аналізу фізико-хімічних властивостей розчинів – метод бінарних адитивних квазісольватів (BAQS). Квазісольват Q_{ij} —гіпотетична двочастинкова структура, в якій одна частинка i є «розчиненою речовиною», а інша частинка j — «розчинником». Набір подібних квазісольватів має макроскопічну властивість F_{ij}. Розчин є адитивною сумішшю квазісольватів з ваговими функціями w_{ij}. У рамках методу BAQS розроблено дві моделі: із симетричними ваговими функціями (BAQS/S) та з асиметричними ваговими функціями (BAQS/A). На прикладі об'ємних властивостей розчинів неелектролітів показано можливості методу. Визначено ефективні граничні парціальні молярні об'єми компонентів для сумішей неелектролітів. Розглянуто можливість прогнозування властивостей багатокомпонентних розчинів за даними для двокомпонентних систем. Показано застосування до інших властивостей розчину. Кожна із запропонованих моделей має свої переваги та недоліки.

BAQS/S: описує молярні об'єми сумішей, особливо для апротонних систем, може бути використана для прогнозування властивостей багатокомпонентних систем, ефективна на невеликих наборах даних. Обмеження: застосовність до інших властивостей розчинів залишається під питанням, параметри моделі відрізняються від отриманих незалежним методом, точність апроксимації поступається емпіричним моделям.

BAQS/A: застосовна для будь-яких властивостей розчину, інформативна та ілюстративна. Обмеження: дуже чутлива до вибору апроксимуючого рівняння, важко інтерпретувати результати, розроблено лише для двокомпонентних систем.

Ключові слова: *фізико-хімічний аналіз, молярний об'єм, граничний парціальний молярний об'єм, рівняння Редліха-Кістера, розчини неелектролітів, багатокомпонентні суміші, бінарні адитивні квазісольвати.*

ЕТИЧНІ НОРМИ ПУБЛІКАЦІЇ НАУКОВИХ РЕЗУЛЬТАТІВ ТА ЇХ ПОРУШЕННЯ. Редакційна колегія робить все можливе для дотримання етичних норм, прийнятих міжнародним науковим товариством, і для запобігання будь-яких порушень цих норм. Така політика є важливою умовою плідної участі журналу в розвитку цілісної системи знань в галузі хімії та суміжних галузях. Діяльність редакційної колегії значною мірою спирається на рекомендації Комітету з етики наукових публікацій (Committee of Publication Ethics), а також на цінний досвід міжнародних журналів та видавництв. Подання статті на розгляд означає, що вона містить отримані авторами нові нетривіальні наукові результати, які раніше не були опубліковані. Кожну статтю рецензують щонайменше два експерти, які мають усі можливості вільно висловити мотивовані критичні зауваження щодо рівня та ясності представлення матеріалу, його відповідності профілю журналу, новизни та достовірності результатів. Рекомендації рецензентів є основою для прийняття остаточного рішення щодо публікації статті. Якщо статтю прийнято, вона розміщується у відкритому доступі; авторські права зберігаються за авторами. За наявності будь-яких конфліктів інтересів (фінансових, академічних, персональних та інших), учасники процесу рецензування мають сповістити редакційну колегію про це. Всі питання, пов'язані з можливим плагіатом або фальсифікацією результатів ретельно обговорюються редакційною колегією, рівно як спори щодо авторства та доцільність роздроблення результатів на невеличкі статті. Доведені плагіат чи фальсифікація результатів є підставами для безумовного відхилення статті.

STATEMENT ON THE PUBLICATION ETHICS AND MALPRACTICE. The Editorial Board has been doing its best to keep the ethical standards adopted by the world scientific community and to prevent the publication malpractice of any kind. This policy is considered to be an imperative condition for the fruitful contribution of the journal in the development of the modern network of knowledge in chemistry and boundary fields. The activity of the Editorial Board in this respect is based, in particular, on the recommendations of the Committee of Publication Ethics and valuable practice of world-leading journals and publishers. The submission of a manuscript implies that it contains new significant scientific results obtained by authors that where never published before. Each paper is peer reviewed by at least two independent experts who are completely free to express their motivated critical comments on the level of the research, its novelty, reliability, readability and relevance to the journal scope. These comments are the background for the final decision about the paper. Once the manuscript is accepted, it becomes the open-access paper, and the copyright remains with authors. All participants of the review process are strongly asked to disclose conflicts of interest of any kind (financial, academic, personal, etc.). Any indication of plagiarism or fraudulent research receives extremely serious attention from the side of the Editorial Board, as well as authorship disputes and groundless subdivision of the results into several small papers. Confirmed plagiarism or fraudulent research entail the categorical rejection of the manuscript.

ІНФОРМАЦІЯ ДЛЯ АВТОРІВ. Журнал публікує статті російською, англійською та українською мовами. До публікації приймаються: огляди (за погодженням з редколегією); оригінальні статті, обсяг 6-10 журнальних сторінок; короткі повідомлення, обсяг до 3 журнальних сторінок. Крім звичайного списку літератури, в статті обов'язково повинен бути другий список, всі посилання якого дані латиницею. Правила підготовки цього списку наведені в розділі «Трансliteraція» на сайті журналу. Обидва списки повинні бути повністю ідентичні. При рецензуванні статей один з критеріїв - наявність посилань на публікації останніх років. Стаття обов'язково повинна містити резюме російською, українською та англійською мовами. У всіх трьох необхідно вказати назву статті, прізвища авторів і ключові слова. Орієнтовний обсяг резюме - 1800 знаків (без урахування заголовку і ключових слів). Редакція приймає електронний (MS Word) і два роздрукованих (для харків'ян) тексту рукопису. Адреси вказані в розділі «Контакти» на сайті журналу. Супровідний лист до статті, виправленої відповідно до зауважень рецензента, повинен містити відповіді на всі зауваження. Подається електронний і один роздрукований (для харків'ян) варіант. Рукописи, які пройшли рецензування, прийняті до публікації і оформлені відповідно до правил для авторів, приймаються у форматі doc (не docx) електронною поштою (chembull@karazin.ua). Роздрукований варіант не потрібен. Докладніша інформація розміщена на сайті журналу http://chembull.univer.kharkov.ua.

INFORMATION FOR AUTHORS. Papers in Ukrainian, Russian and English are published. These may be invited papers; review papers (require preliminary agreement with Editors); regular papers; brief communications. In preparing the manuscript it is mandatory to keep the statement on the publication ethics and malpractice, which can be found on the web-site and in each issue. The article should contain summaries in English, Russian, and Ukrainian. In all three it is necessary to indicate the title of the article, the names of the authors and the keywords. The approximate volume of summary is 1800 characters (excluding the title and key words). The help in translation is provided by request for foreign authors.. Any style of references is acceptable, but all references within the paper must be given in the same style. In addition, the second, transliterated, list of references is required if at least one original reference is given in Cyrillic. See section "Transliteration" of the web-site for details. Please use papers of previous issues as samples when prepare the manuscript. The MS Word format is used. Standard fonts (Times New Roman, Arial, Symbol) are preferable. Figures and diagrams are required in vector formats. Figure captions are given separately. All figures, tables and equations are numbered. Please use MS Equation Editor or MathType to prepare mathematical equations and ISIS Draw to prepare chemical formulas and equations. The decimal point (not coma) is accepted in the journal. Please avoid any kind of formatting when prepare the manuscript. Manuscripts may be submitted to the Editor-in-Chief via e-mai chembull@karazin.ua. For more detailed information see the journal web-site http://chembull.univer.kharkov.ua.

Наукове видання

Вісник
Харківського національного університету
імені В.Н. Каразіна

Серія «Хімія»
Вип. 41 (64)
Збірник наукових праць
Українською та англійською мовами.

Технічний редактор:
Д.О. Анохін